precursor cells residing in the bone marrow and peripheral blood for future clinical applications.

2 Results

2.1 Development of NKT cells from cultures of bone marrow cells

We previously demonstrated that NK1.1$^+$, TCR$\alpha\beta^+$ cells can develop in suspension cultures of mouse fetal liver supplemented with the appropriate cytokines [7]. Several lines of evidence supported that Vα14i NKT cells were one of the main subsets among the NK1.1$^+$, TCR$\alpha\beta^+$ cells in the culture. In the present study, we attempted to use the fetal liver culture system to obtain Vα14i NKT cells from cultures of bone marrow and peripheral blood hematopoietic precursors.

In bone marrow, NKT and conventional T cells account for less than 1% of all mononuclear cells (MNC) (Fig. 1A). When bone marrow MNC were transferred to medium supplemented with cytokines [a combination of culture supernatant from Con A-stimulated T cells (Con A sup), IL-3, IL-4, IL-7 and GM-CSF, see below], both NKT and conventional T cell numbers increased, in contrast to fetal liver culture where preferential differentiation of NKT cells occurred [7]. Considering the difference between bone marrow and fetal liver cell compositions, we speculated that the presence of certain subsets of mature NKT or conventional T cells in the bone marrow culture prevented the differentiation of hematopoietic precursors into NKT cells. Thus, bone marrow cells were treated with magnetic beads coated with anti-Thy-1 antibody to remove mature NKT and T cells before the culture. When Thy-1$^+$-depleted bone marrow cells were cultured in the same medium, preferential differentiation of NKT cells from precursors was observed (Fig. 1A).

NKT cell differentiation from bone marrow precursors was cytokine-dependent. Few NKT cells were generated in cultures without cytokine supplements (Fig. 1A). Culture supernatants from WEHI-3 and EL-4 were used to induce NKT cell differentiation from fetal liver in the previous study [7]. To determine the cytokines included in these supernatants and required for the induction of NKT cells in culture, the blocking effects of anti-cytokine antibodies were examined. The presence of antibodies against IL-2, IL-3, IL-4, IL-7, IFN-γ and GM-CSF but not against SCF was found to inhibit NKT cell development in the culture of Thy-1$^+$-depleted bone marrow cells in the presence of WEHI-3 and EL-4 culture supernatants (data not shown). When Thy-1$^+$-depleted bone marrow cells were cultured in the presence of Con A sup (instead of recombinant IL-2, also available from cultures of human peripheral blood T cells) and recombinant IL-3, IL-4, IL-7 and GM-CSF, NKT cell development at an efficiency comparable to that of the cultures supplemented with WEHI-3 and EL-4 culture supernatants was observed. Taking into account future human applications, a combination of these factors was used as supplements in the present study.

The yield of NKT cells was dependent on the experiment but usually reached ~1×10^5 (from culture of 1×10^7 bone

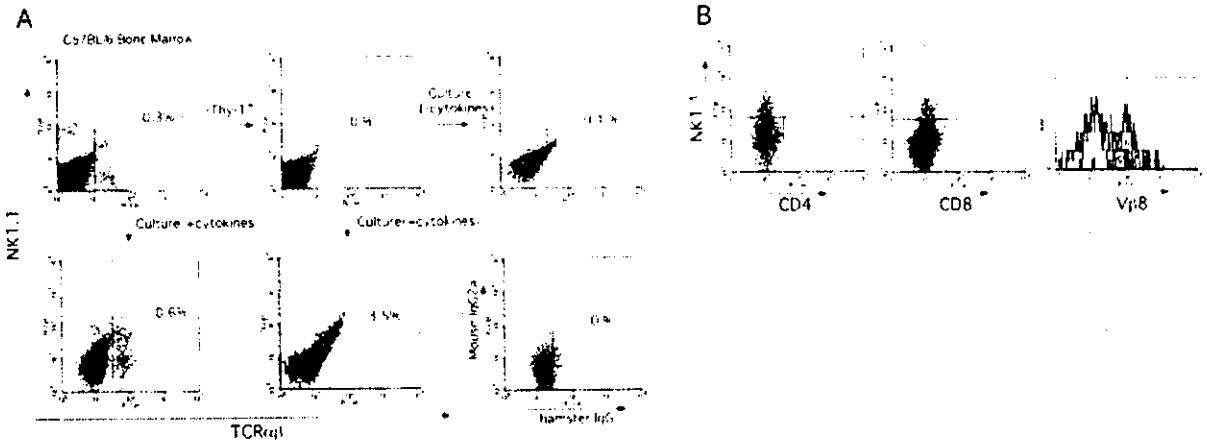

Fig. 1. Development of NKT cells in bone marrow culture. C57BL/6 bone marrow cells before and after depletion of Thy-1$^+$ cells were cultured for 7 days in the presence or absence of cytokines. (A) FACS analysis for expression of NK1.1 and TCR$\alpha\beta$. The percentage of NK1.1$^+$, TCR$\alpha\beta^+$ cells is indicated in each panel. The panel boxed in the broken line indicates staining of Thy-1$^+$-depleted bone marrow cells with fluorescence-labeled isotype-matched control antibodies after culture in the presence of cytokines. (B) Thy-1$^+$-depleted bone marrow cells were analyzed for the expression of CD4, CD8 and TCR Vβ8 after culture with cytokines.

marrow cells), corresponding to 5-fold increase from the number of NKT cells in bone marrow before Thy-1$^+$ cell depletion and culture.

2.2 CD1-dependent Vα14i NKT cell development in bone marrow culture

NKT cells generated in bone marrow cultures had the phenotype CD4$^-$8$^-$ and predominantly used Vβ8 (Fig. 1B). These features correspond well to those of Vα14i NKT cells [1–3]. To further characterize the NKT cells in bone marrow culture, the CD1 dependency of their development was examined. Generation of NKT cells in the culture of CD1$^{-/-}$ bone marrow cells was much less extensive than that in the culture of wild-type bone marrow cells (Fig. 2A). Most NKT cells generated in the wild-type bone marrow culture were stained with tetramer of the CD1–α-galactosylceramide (α-GalCer) complex [(CD1–α-GalCer)$_4$] but not with CD1 tetramers without α-GalCer. In contrast, few cells in the culture of CD1$^{-/-}$ bone marrow cells were stained with the tetramer. CD1-dependent generation of NKT cells in the culture of wild-type bone marrow cells was also supported by the inhibitory effect of anti-CD1 monoclonal antibodies (data not shown). The expression of Vα14 mRNA was found in Thy-1$^+$-depleted bone marrow cells after, but not before culture (Fig. 2B). Collectively, these results indicate that the development of NKT cells in the culture of Thy-1$^+$-depleted bone marrow cells is CD1-dependent and that a significant fraction of these NKT cells are Vα14i NKT cells.

2.3 Reconstitution of NKT cell development from CD1$^{-/-}$ bone marrow precursors in mixed culture with recombination-deficient Rag-2$^{-/-}$ bone marrow cells

NKT cell development from CD1$^{-/-}$ bone marrow cells is suppressed (as shown in Fig. 2A) due to a lack of CD1$^+$ cells responsible for the positive selection of NKT cells, although putative precursor cells are present. We attempted to reconstitute NKT cell development from CD1$^{-/-}$ precursors through interaction with CD1$^+$ selecting cells in order to elucidate the *de novo* differentiation of NKT cells from precursors in the culture. Thy-1$^+$-depleted CD1$^{-/-}$ bone marrow cells were mixed with bone marrow cells from recombination-deficient Rag-2$^{-/-}$ mice (CD1$^+$ but lacking lymphoid development). Mixed bone marrow cultures of CD1$^{-/-}$ and Rag-2$^{-/-}$ mice at an appropriate ratio gave rise to NKT cells in numbers comparable to a C57BL/6 control bone marrow culture (Fig. 3A), and about half of the cells were (CD1–α-GalCer)$_4^+$ Vα14i NKT cells (Fig. 3B). These results confirm that bone marrow contains the precursor cells and that they differentiate into NKT cells in culture upon interaction with CD1$^+$ selecting cells.

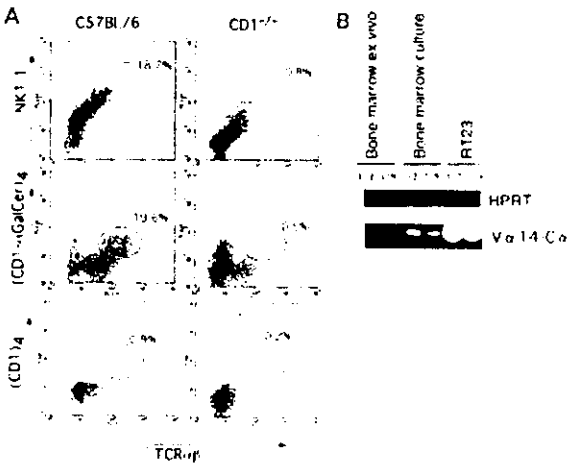

Fig. 2. Development of CD1-dependent Vα14i NKT cells in the culture of bone marrow cells. (A) Staining with (CD1–α-GalCer)$_4$. Thy-1$^+$-depleted bone marrow cells isolated from C57BL/6 or CD1$^{-/-}$ mice were cultured for 7 days in the presence of the cytokine mixture. The cells were analyzed for expression of NK1.1 and TCRαβ (upper panels) or Vα14i TCR using (CD1–α-GalCer)$_4$ or empty CD1 tetramers (CD1)$_4$ and TCRαβ antibody (lower panels). (B) Expression of Vα14-Cα mRNA in Thy-1$^+$-depleted bone marrow cells before and after culture was examined by RT-PCR. A Vα14i$^+$ hybridoma (RT23) was analyzed as a positive control. The amount of cDNA used for template is shown in μg on each lane. The expression of HPRT mRNA was simultaneously analyzed to compare the amount of total mRNA in analysis.

2.4 Development of Vα14i NKT cells from peripheral blood hematopoietic precursors sustained by bone marrow stromal cells

For human applications, peripheral blood is a much more convenient source of hematopoietic precursors than bone marrow. We therefore tried to induce NKT cell differentiation in cultures of peripheral blood cells. Neither selective expansion of NKT cells from a culture of total MNC nor induction of NKT cell differentiation from Thy-1$^+$-depleted peripheral blood MNC was observed (Fig. 4A). Based on these results, it was assumed that in hematopoietic organs (fetal liver, adult bone marrow), certain microenvironments for NKT cell differentiation are present; they contribute to the differentiation of NKT cells from precursors when cells from hematopoietic organs are subjected to suspension culture. We tried to transfer such putative microenvironments for NKT cell differentiation to cell culture. Bone marrow cells were

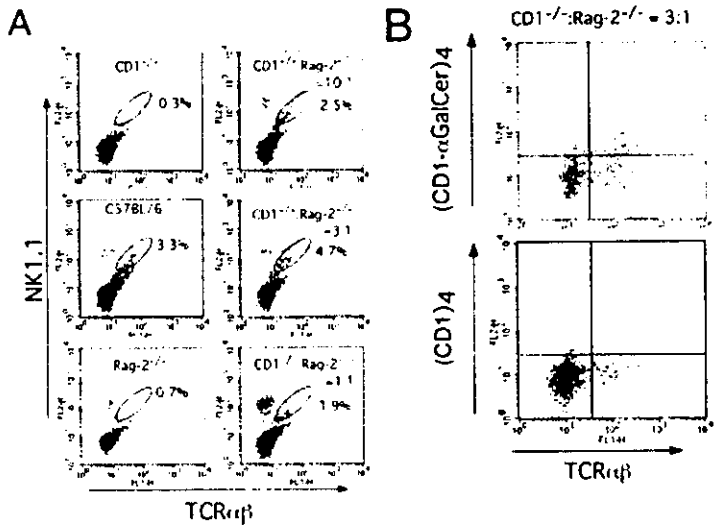

Fig. 3. Reconstitution of the generation of NKT cells from $CD1^{-/-}$ bone marrow hematopoietic precursors by co-culture with bone marrow cells from $CD1^{+/+}$ mice. $CD1^{-/-}$ bone marrow cells were depleted of Thy-1^+ cells and were cultured with or without Rag-$2^{-/-}$ bone marrow cells at the indicated ratio for 7 days. The proportion of NKT cells generated in each culture was determined and compared with that in the culture of Thy-1^+-depleted C57BL/6 bone marrow cells. (A) Development of NK1.1^+, TCR$\alpha\beta^+$ cells was determined by FACS analysis. (B) The cells in the culture of $CD1^{-/-}$ and Rag-$2^{-/-}$ bone marrow cells (3:1) were stained with $(CD1\text{–}\alpha\text{-GalCer})_4$ or empty CD1 tetramers $(CD1)_4$ and TCR$\alpha\beta$ antibody.

cultured in the presence of a mixture of cytokines as described, and the cells that adhered to the culture plate (bone marrow stromal cells) were prepared. The stromal cells were co-cultured with Thy-1^+-depleted peripheral blood MNC. After culture for 7 days, NKT cell development was observed in the culture (Fig. 4A). In this experiment, the bone marrow stromal cells were prepared from recombination-deficient scid mice to ensure that the NKT cells were derived from precursors in the peripheral blood. However, both recombination-deficient and Thy-1^+-depleted normal bone marrow stromal cells of any strain were applicable to the induction of NKT cell differentiation from peripheral blood precursors (data not shown). The yield of NKT cells generated in the culture was improved when peripheral blood was prepared from mice pre-treated with G-CSF (4-fold increase in number) (Fig. 4A). The number of NKT cells in a culture of 1 ml G-CSF-injected peripheral blood ($\sim 1\times10^7$ MNC) was estimated to be 5×10^4, corresponding to 50-fold increase from the number of NKT cells in blood before culture.

The NKT cells in the culture had the phenotype $CD4^-$, $CD8^-$ and V$\beta8^+$, similar to those generated from bone marrow culture (data not shown). Nearly half of the cells stained with $(CD1\text{–}\alpha\text{-GalCer})_4$; tetramer-staining cells were absent when peripheral blood MNC were co-cultured with $CD1^{-/-}$ bone marrow stromal cells (Fig. 4B). Thus, these findings confirm that CD1-dependent Vα14i NKT cells represent one of the major subsets of NKT cells generated in the culture of peripheral blood MNC with $CD1^+$ bone marrow stromal cells.

2.5 Anti-tumor activity of NKT cells generated in culture

To characterize the NKT cells generated in the culture of bone marrow or peripheral blood cells, their cytotoxicity to tumor line cells was examined. NKT cells were induced in culture from Thy-1^+-depleted bone marrow or peripheral blood cells of C57BL/6 or $CD1^{-/-}$ mice as described above and were used as effectors (Fig. 5). The cells cultured from C57BL/6 bone marrow or peripheral blood cells were found to have significant cytotoxic activity against various tumor lines [melanoma line B16 ($H\text{-}2^b$), lymphoma line YAC-1 ($H\text{-}2^a$) and mastocytoma line P815 ($H\text{-}2^d$)]. In contrast, cells cultured from $CD1^{-/-}$ bone marrow or peripheral blood cells were less effective. The cells before culture had virtually no cytotoxicity. These results suggest that NKT cells generated in a CD1-dependent manner in the culture are chiefly responsible for the cytotoxicity against tumor cells. These CD1-dependent NKT cells were ready to exert cytotoxicity without further activation, presumably due to the circumstances under which they were generated.

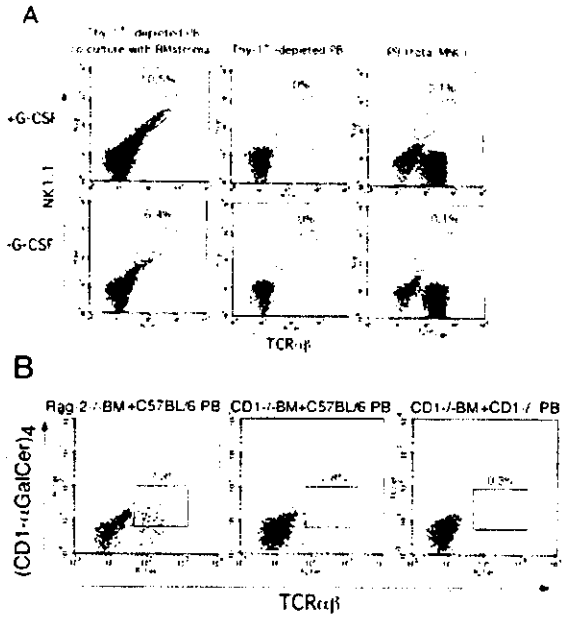

Fig. 4. Development of NKT cells from peripheral blood hematopoietic precursors sustained by bone marrow stromal cells. (A) Thy-1$^+$-depleted peripheral blood MNC were isolated from (G-CSF pre-treated or untreated) C57BL/6 mice. Cells were cultured for 7 days with or without the support of bone marrow stromal monolayers prepared from CB17 scid mice. Development of NK1.1$^+$, TCRαβ$^+$ cells was determined by FACS analysis. (B) Generation of Vα14i NKT cells from peripheral blood precursors. Thy-1$^+$-depleted peripheral blood MNC were prepared from C57BL/6 or CD1$^{-/-}$ mice pre-treated with G-CSF. MNC were co-cultured with stromal cells prepared from Rag-2$^{-/-}$ or Thy-1$^+$-depleted CD1$^{-/-}$ bone marrow cells. After 7 days, cells were analyzed for staining with (CD1–α-GalCer)$_4$ and anti-TCRαβ antibody. (PB, peripheral blood)

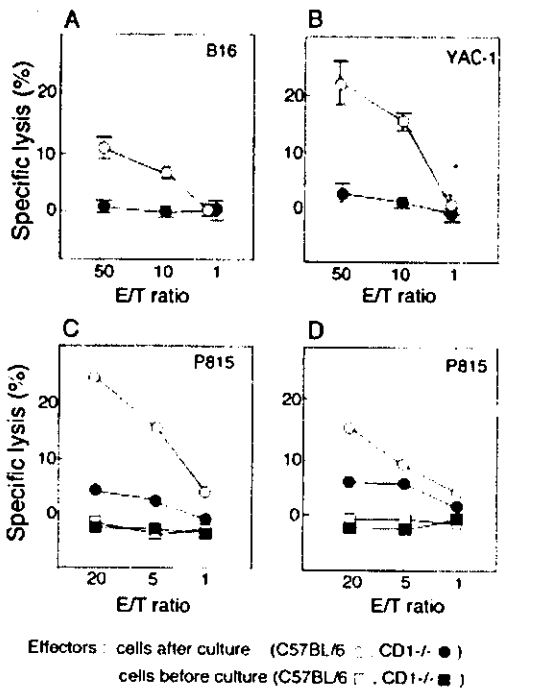

Fig. 5. Cytotoxicity of NKT cells generated in culture. (A–C) Thy-1$^+$-depleted bone marrow cells prepared from C57BL/6 or CD1$^{-/-}$ mice were cultured for 7 days in cytokine-supplemented medium. (D) Thy-1$^+$-depleted peripheral blood MNC prepared from C57BL/6 or CD1$^{-/-}$ mice were co-cultured with bone marrow stromal cells prepared from CB17 scid mice for 7 days. Cells in culture were tested for cytotoxicity against the tumor line cells indicated in each panel. Specific lysis after incubation for 5 h (A, B) or 16 h (C, D) is shown. Uncultured cells were tested in (C) and (D) as a control.

3 Discussion

In the present study, we demonstrate that NKT cells are generated from hematopoietic precursors in cytokine-activated suspension cultures of bone marrow and peripheral blood cells and that one of the major subsets is Vα14i NKT cells, judging from their CD1-dependent generation, expression of Vα14-Jα18 invariant TCR and staining with (CD1–α-GalCer)$_4$. Vα14i NKT cells have been shown to differentiate mainly in the thymus [3–6]. In addition, we proposed minor extrathymic differentiation pathways in the hematopoietic organs, as the presence of Vα14i NKT cells with Vα14-Jα18 junctional sequences peculiar to these organs were observed in the lymphoid organs of athymic mice [8]. Such minor differentiation pathways, if they exist, are presumably controlled to minimum levels under physiological conditions. However, the organized microenvironments for lymphogenesis in the hematopoietic organs might be out of control in suspension cultures of the organs, so that NKT cell development from precursor cells was allowed to proceed.

Taking future applications in humans into account, we used bone marrow and peripheral blood cells as sources of precursors. After the removal of Thy-1$^+$ cells, bone marrow cells were found to be a good source of NKT cell precursors. A possible interpretation of this finding is that the presence of mature NKT cells in culture suppresses NKT cell differentiation from precursors. Another possibility is that certain subsets of T or NKT cells function to inhibit NKT cell differentiation. The level of Thy-1 expression by the putative NKT cell precursors is not clear, but the density of expression was evidently not great enough to cause removal by magnetic beads.

The culture of Thy-1$^+$-depleted peripheral blood cells did not give rise to NKT cells, presumably due to the lack of

putative microenvironments for NKT cell differentiation that are present in the hematopoietic organs. We therefore tested co-cultures of Thy-1$^+$-depleted peripheral blood cells and bone marrow-derived stromal cells and found NKT cell differentiation in the culture. Genetic compatibility between bone marrow stromal cells and peripheral blood precursors was not required, probably because non-polymorphic CD1 expressed by the stromal cells is responsible for the positive selection of NKT cells. This finding indicates that for future clinical applications, self NKT cells can be induced from peripheral blood with the aid of bone marrow stromal cells prepared from healthy donors. Stromal cells from both bone marrow and fetal liver had the ability to induce NKT cell differentiation from peripheral blood precursors (data not shown). However, the stromal cells prepared from these organs retained their inductivity only in the primary culture.

The reconstitution of NKT cell development *in vitro* in co-cultures of CD1$^{-/-}$ and Rag-2$^{-/-}$ bone marrow cells strongly suggests that NKT cell differentiation from precursors, but not selective expansion of remaining NKT cells after Thy-1$^+$ cell depletion, occurred in the culture of bone marrow cells from wild-type mice. Moreover, these findings indicate that the cells responsible for positive selection of NKT cells in the culture are neither of B nor T cell lineage. This is also the case in the induction of NKT cell differentiation from peripheral blood precursors sustained by bone marrow stromal cells; normal and recombination-deficient bone marrow stromal cells induced NKT cell differentiation with essentially the same efficiency (data not shown). Dendritic cells have been suggested to be responsible for the process in fetal liver culture [12].

NKT cells are believed to have important roles in the immune system. Recent reports suggest that NKT cell functions are disturbed in diseases [9–11]. Attempts have been made to increase NKT cell numbers by culturing peripheral blood from patients or to activate NKT cells in patients utilizing the specific activator α-GalCer [13, 14]. The culture system developed in the present study is valid for patients in which NKT cells are decreased in number or functionally disordered but hematopoiesis is still functional. The NKT cells induced in a CD1-dependent manner from precursors *in vitro* are suggested to possess cytotoxicity against tumor cells (Fig. 5). Thus, combination of the culture systems described in this study with the reported methods using α-GalCer will provide new potential for the treatment of patients, especially those suffering from cancer.

4 Materials and methods

4.1 Mice

C57BL/6, BALB/c and CB17 (*scid/scid*) mice were purchased from Sankyo Service Co. (Tokyo, Japan). Rag-2$^{-/-}$ mice were obtained from the Jackson Laboratory (Bar Harbor, ME, USA). CD1$^{-/-}$ mice were provided by Dr. M. J. Grusby (Harvard University) [15] and were partially backcrossed to C57BL/6; mice with the phenotype H-2^b, NK1.1$^+$ and CD1$^{-/-}$ were selected.

4.2 Bone marrow cultures

Cell suspensions of bone marrow from normal or mutant mouse femur and tibia were prepared. Bone marrow cells, with or without treatment with magnetic beads coated with anti-Thy-1 antibody (Dynal Biotech, Oslo, Norway) to remove T and NKT cells, were cultured for 5–10 days in DMEM supplemented with 10% fetal bovine serum, 50 U/ml penicillin, 50 μg/ml streptomycin and 5×10^{-5} M 2-ME. Cultures were further supplemented with Con A sup (5% v/v), recombinant IL-3 (10 ng/ml, Pepro Tech EC, London, GB), IL-4 (0.5 ng/ml, PharMingen, San Diego, CA), IL-7 (5 ng/ml, Pepro Tech EC) and GM-CSF (1 ng/ml, Pepro Tech EC). Con A sup was prepared from rat spleen cells cultured for 2 days in the presence of Con A (5 μg/ml). Con A in the supernatant was removed by Sephadex G-10 column chromatography (Amersham-Pharmacia Biotech, Uppsala, Sweden). Culture supernatants from WEHI-3 and EL-4 (obtained from ATCC, Rockville, MD) were prepared as described [7]. In some experiments, the following anti-cytokine antibodies were added at various concentrations at the initiation of culture: anti-IL-2 (S4B6, PharMingen), anti-IL-3 (goat antiserum, Santa Cruz Biotechnology, CA), anti-IL4 (BVD4, PharMingen), anti-IL-7 (goat antiserum, Santa Cruz Biotechnology), anti-IFN-γ (R4–6A2, PharMingen), anti-GM-CSF (goat antiserum, Santa Cruz Biotechnology) and anti-SCF (goat antiserum, Santa Cruz Biotechnology).

4.3 Peripheral blood cultures

Some mice were injected with G-CSF (0.3 μg/animal, Pepro Tech EC) 3 days before bleeding. MNC were separated from the heparinized peripheral blood of G-CSF-treated and untreated mice by density gradient centrifugation using Lymphosepar II (*d*=1.090, IBL, Gunma, Japan). MNC were then treated with magnetic beads coated with anti-Thy-1 antibody (Dynal), and the remaining cells were transferred to culture on bone marrow stromal cell monolayers. Bone marrow stromal cells were prepared from bone marrow cells cultured as described above. On the 7th day of the culture, the suspended cells were completely removed by suction. The remaining cells (attached to the culture plate) were washed with cold PBS solution and used as bone marrow stromal

monolayers. Thy-1⁺-depleted peripheral blood MNC were co-cultured with bone marrow stromal monolayers for 7–10 days in DMEM supplemented with Con A sup (5%, v/v).

4.4 Preparation of tetramer of CD1–α-GalCer complex

$(CD1–α-GalCer)_4$ was prepared as described by Sidobre et al. [16]. The baculovirus expression vector for CD1-β2-microglobulin synthesis was provided by Dr. Kronenberg (La Jolla Institute). Biotinylated CD1-β2-microglobulin complex was coupled with PE-labeled streptavidin (PharMingen) to make a tetramer of the complex. α-GalCer [(2*S*, 3*R*)-1-*O*-(α-D-galactopyranosyl)-2-(*N*-octadecanoylamino)-1,3-octadecanediol] was synthesized by glycosylation of azidosphingosine, followed by conversion of azido group to acyl amide as will be described elsewhere (Okamoto et al., manuscript in preparation). The $(CD1–α-GalCer)_4$ prepared in our laboratory was confirmed to specifically stain Vα14i NKT cells by FACS analyses of C57BL/6 liver lymphocytes and Vα14i TCR-expressing hybridomas [17] (data not shown).

4.5 Flow cytometry and antibodies

Cells were treated with rat IgG2b monoclonal antibody 2.4 G2 (anti-mouse FcγR II, III) to saturate FcR binding and then treated with non-labeled isotype-matched immunoglobulins for immunostaining. For $(CD1–α-GalCer)_4$ staining, cells were pre-treated with non-labeled CD1 monomer proteins. Specific staining was performed with a combination of the following conjugated monoclonal antibodies and $(CD1–α-GalCer)_4$: H57-597 (anti-mouse TCR Cβ, PharMingen), PK136 (anti-mouse NK1.1, PharMingen), GK1.5 (anti-mouse CD4, PharMingen), 53–6.7 (anti-mouse CD8, PharMingen) and F23.1 (anti-mouse TCR Vβ8, PharMingen). The stained cells were analyzed on a FACScan flow cytometer equipped with Cell Quest software (Becton Dickinson, San Jose, CA).

4.6 RT-PCR

Total RNA was extracted from bone marrow cells before and after culture and from cells of the Vα14i TCR⁺ hybrid line RT23 [17]. cDNA was prepared from total RNA using RT-PCR kits (Takara, Tokyo, Japan). RT-PCR were performed using the following primers: (5'Vα14) 5'-TCCTGGTTGACCAAAAAGAC-3' [18]; (3'Cα) 5'-TGGCGTTGGTCTCTTTGAAG-3' [19]; [5'-hypoxanthine phosphoribosyltransferase (HPRT)] 5'-GTTGAATACAGGCCAGACTTTGTTG-3'; (3'-HPRT) 5'-GAGGGTAGGCTGGCCTATAGGCT-3'.

4.7 Cytotoxicity assay

Cells recovered from the cultures of bone marrow and peripheral blood were assayed for their activity to induce lysis of tumor cells. Viable cells (including ~5% NKT cells) were separated by Lymphosepar II density gradient centrifugation and used as effectors. Target cells [a mastocytoma line P815 ($H-2^d$), a lymphoma line YAC-1 ($H-2^a$) and a melanoma line B16 ($H-2^b$)] were labeled with [^{51}Cr]-sodium chromate (9.25 MBq/ml) for 1 h and cultured with the effector cells at serial ratios for the indicated period of time at 37°C. The release of ^{51}Cr from lysed target cells was quantified with a γ-counter. The percent specific ^{51}Cr-release was calculated using the following formula: percent specific lysis = (sample cpm – spontaneous cpm) × 100/(maximum cpm – spontaneous cpm). Spontaneous cpm was calculated using the supernatant of the target cells alone, and the maximum release was obtained by adding 1% NP40 to target cells.

Acknowledgements: The authors thank Dr. M. J. Grusby (Harvard University) for providing them with $CD1^{-/-}$ mice. They also thank Dr. M. Kronenberg (La Jolla Institute) for the CD1–β2-microglobulin construct. They acknowledge Dr. Yokoyama and his colleagues (Mitsubishi Kagaku Institute of Life Sciences) for taking care of the animals. They also thank Ms. Y. Murakami for preparing the manuscript.

References

1 **Bendelac, A., Rivera, M. N., Park, S. H. and Roark, J. H.,** Mouse CD1-specific NK1 T cells: development, specificity, and function. *Annu. Rev. Immunol.* 1997. **15:** 535–562.

2 **Godfrey, D. I., Hammond, K. J. L., Poulton, L. D., Smyth, M. J. and Baxter, A. G.,** NKT cells: facts, functions and fallacies. *Immunol. Today* 2000. **19:** 362–368.

3 **MacDonald, H. R.,** Development and selection of NKT cells. *Curr. Opin. Immunol.* 2002. **14:** 250–254.

4 **Gapin, L., Matsuda, J. L., Surh, C. D. and Kronenberg, M.,** NKT cells derive from double-positive thymocytes that are positively selected by CD1d. *Nat. Immunol.* 2001. **2:** 971–978.

5 **Benlagha, K., Kyin, T., Beavis, A., Teyton, L. and Bendelac, A.,** A thymic precursor to the NK T cell lineage. *Science* 2002. **296:** 553–555.

6 **Pellicci, D. G., Hammond, K. J. L., Uldrich, A. P., Baxter, A. G., Smyth, M. J. and Godfrey, D. I.,** A natural killer T (NKT) cell developmental pathway involving a thymus-dependent NK1. 1^- $CD4^+$ CD1d-dependent precursor stage. *J. Exp. Med.* 2002. **195:** 835–844.

7 **Shimamura, M., Ohteki, T., Launois, P., Garcia, A.-M. and MacDonald, H. R.,** Thymus-independent generation of $NK1^+$ T cells *in vitro* from fetal liver precursors. *J. Immunol.* 1997. **158:** 3682–3689.

8 **Shimamura, M., Miura-Ohnuma, J. and Huang, Y-Y.,** Major sites for the differentiation of $Vα14^+$ NKT cells inferred from the V-J junctional sequences of the invariant T cell receptor α chain. *Eur. J. Biochem.* 2001. **268:** 56–61.

9 **Wilson, S. B., Kent, S. C., Patton, K. T., Orban, T., Jackson, R. A., Exley, M., Porcelli, S., Schatz, D. A., Atkinson, M. A., Balk, S. P., Strominger, J. L. and Hafler, D. A.,** Extreme Th1 bias of invariant Vα24JαQ T cells in type I diabetes. *Nature* 1998. **391:** 177–181.

10 **Kojo, S., Adachi, Y., Keino, H., Taniguchi, M. and Sumida, T.,** Dysfunction of T cell receptor AV24AJ18$^+$, BV11$^+$ double-negative regulatory natural killer T cells in autoimmune diseases. *Arthritis Rheum.* 2001. **44:** 1127–1138.

11 **Yanagisawa, K., Seino, K., Ishikawa, Y., Nozue, M., Todoroki, T. and Fukao, K.,** Impaired proliferative response of Vα24 NKT cells from cancer patients against α-galactosylceramide. *J. Immunol.* 2002. **168:** 6494–6499.

12 **Shimamura, M., Huang,Y.-Y., Suda, Y., Kusumoto, S., Sato, K., Grusby, M. J., Sato, H., Nakayama, T. and Taniguchi, M.,** Positive selection of NKT cells by CD1$^+$, CD11c$^+$ non-lymphoid cells residing in the extrathymic organs. *Eur. J. Immunol.* 1999. **29:** 3962–3970.

13 **Takahashi, T., Nieda, M., Koezuka, Y., Nicol, A., Porcelli, S. A., Ishikawa, Y., Tadokoro, K., Hirai, H. and Juji, T.,** Analysis of human Vα24$^+$ CD4$^+$ NKT cells activated by α-galactosylceramide-pulsed monocyte-derived dendritic cells. *J. Immunol.* 2000. **164:** 4458–4464.

14 **Motohashi, S., Kobayashi, S., Ito, T., Magara, K. K., Mikuni, O., Kamada, N., Iizasa, T., Nakayama, T., Fujisawa, T. and Taniguchi, M.,** Preserved IFN-α production of circulating Vα24 NKT cells in primary lung cancer patients. *Int. J. Cancer.* 2002. **102:** 159–165.

15 **Smiley, S. T., Kaplan, M. H. and Grusby, M. J.,** Immunoglobulin E production in the absence of interleukin-4-secreting CD1-dependent cells. *Science* 1997. **275:** 977–979.

16 **Sidobre, S. and Kronenberg, M.,** CD1 tetramers: a powerful tool for the analysis of glycolipid-reactive T cells. *J. Immunol. Methods* 2002. **268:** 107–121.

17 **Shimamura, M., Ohteki, T., Beutner, U. and MacDonald, H. R.,** Lack of directed Vα14-Jα281 rearrangements in NK1$^+$ T cells. *Eur. J. Immunol.* 1997. **27:** 1576–1579.

18 **Makino, Y., Yamagata, N., Sasho, T., Adachi, Y., Kanno, R., Koseki, H., Kanno, M. and Taniguchi, M.,** Extrathymic development of Vα14-positive T cells. *J. Exp. Med.* 1993. **177:** 1399–1408.

19 **Casanova, J.-L., Romero, P., Widmann, C., Kourilsky, P. and Maryanski, J. L.,** T cell receptor genes in a series of class I major histocompatibility complex-related cytotoxic T lymphocyte clones specific for a *Plasmodium berghei* nonapeptide: implications for T cell allelic exclusion and antigen-specific repertoire. *J. Exp. Med.* 1991. **174:** 1371–1383.

Correspondence: Michio Shimamura, Developmental Immunology Unit, Mitsubishi Kagaku Institute of Life Sciences, 11 Minamiooya, Machida, Tokyo 194–8511, Japan
Fax: +81-427-246317
e-mail: michio@libra.ls.m-kagaku.co.jp

PAPER

Chronic inflammatory demyelinating polyneuropathy: decreased claudin-5 and relocated ZO-1

T Kanda, Y Numata, H Mizusawa

See end of article for authors' affiliations

Correspondence to: Dr T Kanda, Department of Neurology and Neurological Science, Tokyo Medical and Dental University Graduate School, 1-5-45 Yushima, Bunkyo-ku, Tokyo 113-8519, Japan; t-kanda.nuro@tmd.ac.jp

Received 11 August 2003
In revised form 29 September 2003
Accepted 30 September 2003

J Neurol Neurosurg Psychiatry 2004;**75**:765–769. doi: 10.1136/jnnp.2003.025692

Objectives: To clarify the dynamics of molecules composing the blood–nerve barrier (BNB) in inflammatory neuropathies.
Methods: The expression of four tight junction (TJ) proteins—claudin-1, claudin-5, occludin, and ZO-1—was analysed immunohistochemically in sural nerve biopsy specimens obtained from patients with chronic inflammatory demyelinating polyradiculoneuropathy (CIDP).
Results: Claudin-1 was detected only in perineurial cells, whereas claudin-5 was present in endothelial cells, irrespective of vessel location or size. Occludin and ZO-1 were found in perineurial cells, in addition to some epineurial and endoneurial endothelial cells. In CIDP, percentages of endoneurial small vessels immunoreactive for claudin-5 were significantly decreased, as were ZO-1 immunoreactive endoneurial small vessels, with staining localised to interfaces between cells. Claudin-1 and occludin immunoreactivity did not differ appreciably between the neuropathies examined.
Conclusions: The downregulation of claudin-5 and altered localisation of ZO-1 seen in CIDP specimens may indicate that BNB derangement occurs in inflammatory neuropathies. Further investigation of TJ molecules may suggest new treatments based on properties of the BNB.

Endothelial cells in the adult central nervous system (CNS) and also in the peripheral nervous system (PNS) are coupled by tight junctions (TJ) that resemble those of epithelial barriers[1 2] and show extremely low permeability. Breakdown of these TJs in the blood–nerve barrier (BNB) may allow antimyelin antibodies and various inflammatory cytokines to enter peripheral nerve tissues, exacerbating peripheral nerve injury in inflammatory neuropathies, including Guillain-Barré syndrome[3] and chronic inflammatory demyelinating polyneuropathy (CIDP). The development of new therapeutic strategies to restore BNB function based on the properties of TJs has long has been awaited. Understanding of the molecular basis of TJs has been increasing since 1993, when occludin, a protein with four transmembrane domains, was discovered.[4] Occludin has also been detected in endothelial cells forming the blood–brain barrier (BBB).[5] Occludin deficient cells have been found to form morphologically normal TJs.[6] However, a new family of TJ proteins, claudins, has received attention more recently. Claudins also have four transmembrane domains, but do not show homology to occludin.[7 8] Among claudin family members, claudin-1, claudin-5, and claudin-11 have been demonstrated in the brain.[7 8] Because claudin-11 is expressed only in oligodendrocytes,[9] and presumably is not related to endothelial barriers, we focused on claudin-1 and claudin-5 as molecules of interest concerning the barrier system in both the CNS and PNS. In our present study, using immunohistochemistry, we analysed the expression of four representative TJ proteins—claudin-1, claudin-5, occludin, and ZO-1—in the human PNS using sural nerve biopsy specimens. We examined the expression of these molecules in PNS disorders in which BNB breakdown is believed to have an important pathogenetic role.

MATERIALS AND METHODS

Patients

Sural nerve biopsy specimens obtained from 25 patients including 10 from patients with CIDP (eight men and two women; age range, 13–64 years; mean, 44.3) were studied. Informed consent was obtained from each patient. The study complied with the ethical guidelines of Tokyo Medical and Dental University. Diagnoses were based on detailed clinical and electrophysiological investigations of the patients, in addition to the pathological examination of sural nerve specimens, including toluidine blue stained semithin sections and teased fibre preparations. CIDP was diagnosed according to standard criteria,[10] and all 10 patients were categorised as "definite" CIDP. Table 1 lists the clinical features and immunostaining results in the patients with CIDP. Other nerve biopsy specimens studied as disease controls included those obtained from six patients with vasculitic neuropathy associated with the Churg-Strauss syndrome (three men and three women; age range, 44–67 years; mean, 57.2); six with hereditary neuropathy (three men and three women; age range, 17–61 years; mean, 45.5; five with type I Charcot-Marie tooth disease and one with hereditary sensory and autonomic neuropathy type II); and four with nutritional neuropathy resulting from vitamin B_1 deficiency (three men and one woman; age range, 23–62 years; mean, 45.8). Specimens were snap frozen and stored at −80°C until use.

Immunohistochemical techniques

Rabbit polyclonal antibodies against human claudin-1, claudin-5, occludin, and ZO-1 were purchased from Zymed (South San Francisco, California, USA). Serial transverse sections (10 μm thick) were cut from specimens on a cryostat, fixed in acetone at 4°C for five minutes, and then exposed to 0.03% H_2O_2/methanol for 10 minutes at room temperature. Sections were then preincubated in phosphate buffered saline (PBS) supplemented with 10% normal goat serum for three hours before incubating overnight with

Abbreviations: BBB, blood–brain barrier; BMEC, brain microvascular endothelial cell; BNB, blood–nerve barrier; CNS, central nervous system; CIDP, chronic inflammatory demyelinating polyneuropathy; PBS, phosphate buffered saline; PNS, peripheral nervous system; TJ, tight junction; VEGF, vascular endothelial growth factor

Table 1 Clinical features and immunostaining results in 10 patients with chronic inflammatory demyelinating polyradiculoneuropathy

Patient	Age/sex	Biopsy (months)	CSF protein (mg/l)	Symptoms	Course	Nerve conduction findings	Antiganglioside antibodies	Anti-C5+ microvessels (%)	ZO-1+ vessels positive at endothelial cell interfaces (%)
1	13 M	10	1170	Mo>Se	Progr	D	–	27.4	57.1
2	24 M	6	960	Mo=Se	Progr	D	–	70.9	11.1
3	31 M	3	1670	Mo=Se	Progr	D	–	38.4	40.0
4	32 F	4	880	Mo=Se	Progr	D+A	GM1 (IgM)	69.4	78.1
5	41 M	5	680	Mo=Se	RR	D	GM1, GD1b, SGPG	72.6	85.7
6	55 F	2	1140	Mo=Se	Progr	D	–	93.2	†
7	58 M	6	1100	Mo<Se	Progr	D	SGLPG	52.2	41.1
8	62 M	3	1610	Mo<Se	RR	D	–	94.5	13.3
9	63 M	72+	9520	Mo=Se	Progr	D	–	63.2	33.3
10	64 M	2	1850	Mo=Se	RR	D	SGLPG	24.3	55.6

*Percentage of ZO-1 immunoreactive endoneurial vessels showing immunoreactivity at endothelial cell interfaces; †ZO-1 immunoreactivity was too faint for the percentage of vessels showing immunoreactivity at endothelial cell interfaces to be evaluated.
Age, age at the time of biopsy; Biopsy, months from disease onset to biopsy; CSF, cerebrospinal fluid; C5, claudin-5; Mo, motor symptoms; Se, sensory symptoms; Course, clinical course until biopsy; Progr, progressive; RR, relapsing and remitting; D, demyelinating; A, axonal; SGPG, sulfoglucuronosyl paraglycoside; SGLPG, sulfoglucuronosyl lactosaminyl paraglycoside.

primary antibody diluted in PBS. Anti-claudin-5 and anti-occludin antibodies were used at a 1/400 dilution, whereas others were used at a 1/800 dilution. Sections were then rinsed with PBS three times before incubation for one hour with peroxidase conjugated secondary antibody (Nichirei, Tokyo, Japan). The reaction product indicating immunoreactivity in sections was developed with diaminobenzidine.

Analysis of claudin-5 positive microvasculature

We analysed endoneurial microvessels less than 30 μm in diameter, which included capillaries and some precapillary arterioles and postcapillary venules. Vessels apparently surrounded by perineurial cell layers were excluded. Because microvessels in the endoneurium were difficult to count accurately in cryostat sections, whether haematoxylin and eosin stained or immunostained using endothelial markers, such as anti-von Willebrand antigen, we first counted these vessels using toluidine blue stained, plastic embedded semithin sections to evaluate the density of endoneurial microvessels/mm^2. The percentage of claudin-5-positive endoneurial microvessels was calculated as the density of anti-claudin-5 immunoreactive microvessels in cryostat sections ×100/overall density of microvessels in toluidine blue stained sections. If the first density exceeded the last, the percentage of claudin-5 immunoreactive microvessels was considered to be 100%. More than 0.5 mm^2 surface area of endoneurial space was evaluated in each specimen.

Analysis of staining pattern by anti-ZO-1 antibody

The percentage of endoneurial microvessels showing ZO-1 immunoreactivity localised at interfaces between adjoining endothelial cells was evaluated. Microvessels showing two or more immunoreactive lines across the endothelial cell layer, or two or more immunoreactive dots located at the luminal side of endothelial cells (fig 1) were judged to have ZO-1 localised at these endothelial cell borders. The percentage of ZO-1 immunoreactive cells with this localisation pattern was calculated as the number of endoneurial microvessels showing linear or punctate ZO-1 immunoreactivity at borders between endothelial cells ×100/overall number of ZO-1 immunoreactive endoneurial microvessels.

RESULTS

Claudin-1 immunoreactivity was evenly present in the perineurial cell layers, with no clear difference in immunoreactivity between the inner and outer layers. No specimen showed staining of endothelial cells (figs 2A and 3). No difference in claudin-1 immunoreactivity was noted between CIDP and the other disease groups (fig 3).

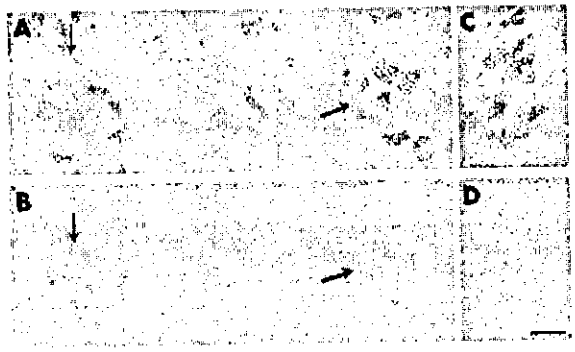

Figure 1 Immunostaining with anti-ZO-1 antibody (B and D) and corresponding serial sections (A and C; haematoxylin and eosin staining) in sural nerves from a 67 year old woman with Churg-Strauss syndrome (A and B) and a 58 year old man with chronic inflammatory demyelinating polyneuropathy (CIPD) (C and D). ZO-1 immunoreactivity in endoneurial microvessels was localised to the interfaces between endothelial cells (arrows), especially at the luminal surface (note the punctate staining of the microvessel on the left in B). In CIDP, endothelial immunoreactivity was diffuse and weak (D); most strong staining localised to the intercellular borders had disappeared. Bar, 10 μm.

The polyclonal anti-occludin antibody stained the perineurial cell layers. In addition, the luminal aspect of some epineurial vessels and a small proportion of endoneurial capillaries adjacent to the perineurium was also immunoreactive (fig 2B). Endoneurial microvessels situated near the centre of the endoneurial space that were not neighbouring perineurial cell layers were not stained. No appreciable difference in immunoreactivity was noted between CIDP and the other disease groups.

Anti-ZO-1 immunoreactivity was localised to the perineurial cell layers, in addition to some endothelial cells lining epineurial vessels and the endoneurium (fig 2C). Although no detectable background staining was seen with the anti-occludin, anti-claudin-1, and anti-claudin-5 antibodies, faint background immunoreactivity was occasionally seen in the endoneurium with the anti-ZO-1 antibody. Therefore, the exact percentage of stained endoneurial microvessels was difficult to determine. Instead, we calculated the percentage of endoneurial microvessels showing immunoreactivity localised to the junctions between endothelial cells (fig 1). In CIDP specimens, the percentage of endoneurial microvessels

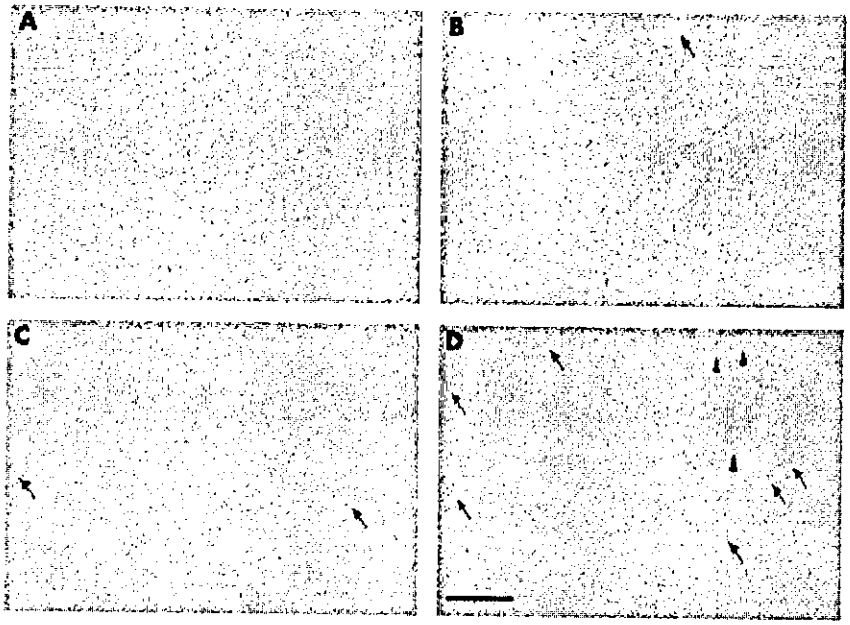

Figure 2 Immunostaining in serial sections obtained from a 64 year old man with Churg-Strauss syndrome with (A) anti-claudin-1, (B) anti-occludin, (C) anti-ZO-1, and (D) anti-claudin-5 antibodies, showing a normal pattern of staining in the human peripheral nervous system. (A) Anti-claudin-1 antibody stained perineurial cell layers exclusively, with no immunoreactivity against endothelial cells. (B) Anti-occludin immunoreactivity was noted in perineurial cell layers. In addition, faint staining was seen in the endothelial cell layers of epineurial vessels (arrow). (C) The anti-ZO-1 antibody reacted faintly with epineurial cell layers and some of the endothelial cells in the endoneurium (arrows). (D) Unlike the other three antibodies, anti-claudin-5 antibody stained endothelial cells exclusively, irrespective of their vessel size or location. Endothelial cells in the epineurium (arrowheads) and in the endoneurium (arrows) were immunoreactive. Bar, 100 μm.

with such anti-ZO-1 immunoreactivity localisation was significantly lower (fig 4).

Claudin-5 was detected exclusively in endothelial cells, irrespective of the location or size of the vessel in the control specimen (figs 2D and 5). Unlike anti-ZO-1 immunostaining, immunoreactivity was not detected at endothelial cell interfaces. In CIDP, the percentage of anti-claudin-5 immunoreactive microvessels in the endoneurium was significantly decreased compared with non-inflammatory neuropathies (figs 5 and 6). No apparent correlation was noted between the loss of claudin-5 immunoreactivity and endoneurial/subperineurial oedema

DISCUSSION

In inflammatory neuropathies including CIDP, increases in cytokines such as interleukin 1β,[11 12] tumour necrosis factor α,[11 12] and vascular endothelial growth factor (VEGF)[13] are believed to contribute to pathogenesis through modulation of the BNB. Among these, VEGF acts as a particularly potent disrupter of the BNB in various inflammatory neuropathies.[14] This increase in vascular permeability occurs through the binding of VEGF to its tyrosine kinase-type receptors, flt-1 and flt-k,[15] resulting in a decrease in TJ proteins, including occludin and vascular endothelial cadherin, and subsequent disorganisation of interendothelial cell junctions.[16] Thus, study of the molecular dynamics of TJ proteins in human inflammatory neuropathies may improve understanding of BNB derangement and prompt the development of new therapeutic approaches in these disorders. Recent experiments have indicated that the establishment of TJ strands depends on claudin family proteins. For example, the transfection of claudin-1 and claudin-2 into fibroblasts induces the formation of TJ strands.[17] Claudin-11 knockout

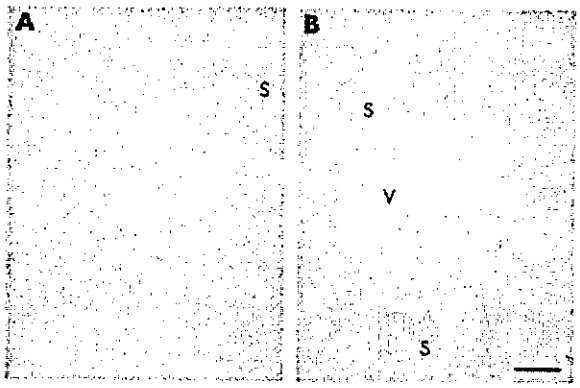

Figure 3 Claudin-1 immunostaining in a control specimen from (A) a 67 year old woman with Churg-Strauss syndrome (CSS) and (B) a specimen from a 55 year old woman with chronic inflammatory demyelinating polyneuropathy (CIDP). Claudin-1 immunoreactivity was detected exclusively in the perineurial cell layers, and no endothelial staining was noted in the endoneurium or epineurium (V). Sections from CIDP and CSS were stained equally. V designates a medium sized epineurial vessel and S designates small sized nerve fascicles. Bar, 100 μm.

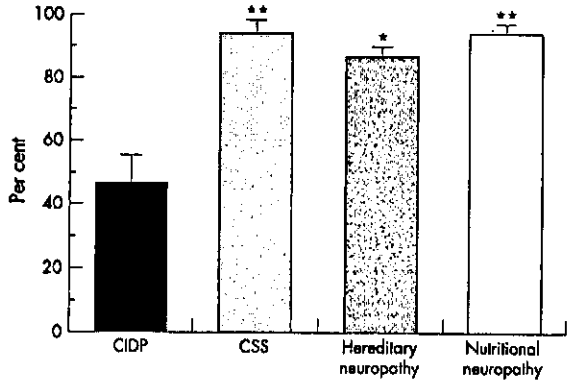

Figure 4 Mean percentage of all ZO-1 immunoreactive endoneurial microvessels showing localisation of ZO-1 immunoreactivity to the interfaces between endothelial cells in specimens with chronic inflammatory demyelinating polyneuropathy (CIDP) (mean, 46.1%; SEM, 8.6%), Churg-Strauss syndrome (CSS) (mean, 93.8%; SEM, 3.7%), hereditary neuropathy (mean, 86.3%; SEM, 3.1%), and nutritional neuropathy (mean, 94.0%; SEM, 2.1%). CIDP specimens showed a significantly lower percentage of endoneurial microvessels with this localisation of ZO-1 immunoreactivity. *$p < 0.005$ *v* CIDP; **$p < 0.002$ *v* CIDP. Bars indicate SEM.

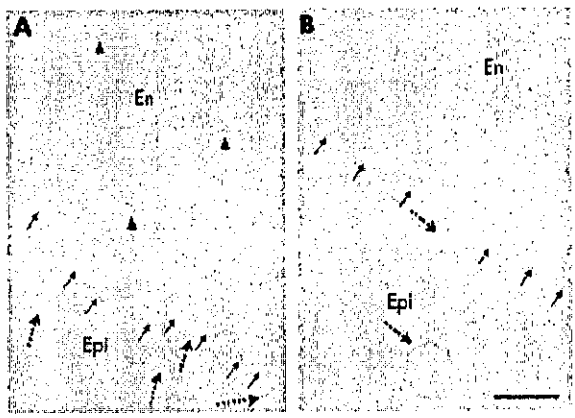

Figure 5 Claudin-5 immunostaining in (A) a control specimen from a 67 year old woman with Churg-Strauss syndrome and (B) a 31 year old man with chronic inflammatory demyelinating polyneuropathy (CIDP). The small arrows indicate the outer aspect of the endoneurium. In the control (A), claudin-5 immunoreactivity was detected exclusively in endothelial cells, irrespective of vessel size or location. Dotted arrows indicate immunoreactive microvessels in the epineurium and arrowheads indicate those in the endoneurium. In CIDP (B), although medium sized vessels in the epineurium were well stained (dotted arrows), immunoreactivity in the endoneurium was severely decreased. En, endoneurium; Epi, epineurium. Bar, 50 μm.

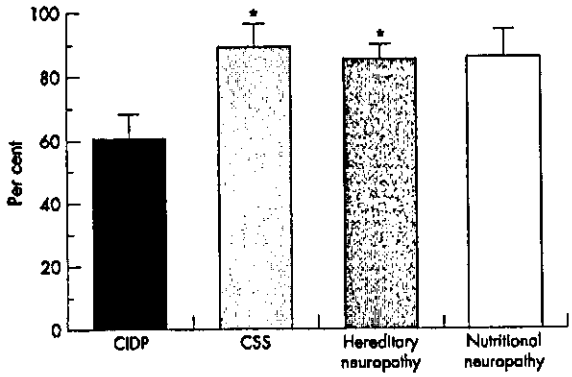

Figure 6 Mean percentage of endoneurial microvessels immunoreactive with anti-claudin-5 antibody in specimens with chronic inflammatory demyelinating polyneuropathy (CIDP) (mean, 60.6%; SEM, 7.8%), Churg-Strauss syndrome (CSS) (mean, 89.5%; SEM, 6.5%), hereditary neuropathy (mean, 85.6%; SEM, 4.0%), and nutritional neuropathy (mean, 86.2%; SEM, 8.4%). Staining with the anti-claudin-5 antibody in the endothelial cells of the endoneurium was significantly decreased in CIDP specimens compared with CSS and hereditary neuropathy. *$p < 0.05$ v CIDP. Bars indicate SEM.

mice show absence of TJ strands in the myelin sheets of oligodendrocytes and Sertoli cells,[16] whereas claudin-16 knockout mice demonstrate abnormal paracellular passage of Mg^{2+} ions.[19] Accordingly, we first focused on the expression of two claudin family members, claudin-1 and claudin-5, in sural nerve biopsy specimens.

Claudin-5, which localises exclusively to borders between adjacent endothelial cells,[20] is considered to be important in the control of vascular permeability. Recently Nitta *et al* reported the selective leakage of small molecules (< 800 Da) across the BBB in claudin-5 deficient mice.[21] This suggests that claudin-5, although ubiquitously present in all endothelial cells, plays a special role in the barrier mechanism of the nervous system by preventing the entrance of such small molecules. In their article, no information was given about the BNB, but free entrance of small molecules through claudin-5 deficient endothelial junctions may also occur in the PNS. Hence, the loss of claudin-5 in the endoneurial microvessels in patients with CIDP may enhance the leakage of small molecules into the endoneurial space, and may result in changes to the endoneurial constituents that are unfavourable to Schwann cells and axons, eventually leading to the worsening of neuropathy. However, we found no correlation between the loss of claudin-5 immunoreactivity and the presence of endoneurial/subperineurial oedema; in addition, $Cld5^{-/-}$ mice do not show vasogenic oedema. This might be explained by the fact that even in claudin-5 deficiency most serum proteins (molecular mass > 800 Da) cannot extravasate.[21] Endoneurial/subperineurial oedema, a relatively common finding in sural nerve specimens from patients with CIDP,[22] may be elicited by factors other than a decrease in claudin-5 expression.

The disagreement between our BNB findings and previous observations concerning the BBB[20] is somewhat difficult to account for; one explanation is that downregulation of claudin-5 in endoneurial microvessels in CIDP might be a BNB specific phenomenon, reflecting differences in anatomic structure and cell populations (for example, the absence of astrocytes). Of 10 CIDP specimens, two (from patients 6 and 8) showed normal anti-claudin-5 immunoreactivity in endoneurial microvessels; this could reflect a non-uniform or multifocal, rather than diffuse, distribution of demyelinative foci in this disorder.[23] However, these two specimens showed extremely faint ZO-1 immunoreactivity (patient 6) or a very low percentage of endoneurial vessels showing ZO-1 immunoreactivity at intercellular interfaces (patient 8). Thus, changes of expression of claudin-5 and ZO-1 are not always in parallel with CIDP, suggesting functional differences between these two TJ proteins.

Although claudin-1 is the only member of the claudin family (except for claudin-5) that might be expected to be present in endothelial cells, we found no staining for claudin-1 in the endothelial cells of the PNS. Instead, the anti-claudin-1 antibody exclusively stained the perineurial cell layers. Because the BNB includes the endoneurial microvasculature and the innermost layer of the perineurium,[24 25] anti-claudin-1 immunoreactivity might be taken to represent the latter. However, the uniform staining of all perineurial cell layers that was seen does not correspond well to the site of the BNB. In addition, claudin-1 immunoreactivity was almost as abundant in CIDP as in control specimens. Therefore, claudin-1 is not a marker of BNB integrity.

In our present study, we detected occludin immunoreactivity in endothelial cells of some epineurial vessels, a small percentage of endoneurial capillaries adjoining perineurial cell layers, and perineurial cells. However, we saw no appreciable differences in occludin immunoreactivity in the perineurial cell layer and in the endothelial cells between the various disorders. Occludin may not be essential for TJ formation,[6] but it has been reported to be abundant in relation to the endothelial cells of the brain, although it is undetectable in non-neural tissues.[3 26] VEGF treatment of brain microvascular endothelial cell (BMEC) monolayer cultures decreased detectable occludin and disrupted its continuous pericellular distribution.[27] Although these reports suggest that occludin may play some part in the maintenance of BNB integrity, our results indicated that occludin does not change appreciably in inflammatory neuropathies.

ZO-1, a 220 kDa TJ phosphoprotein, is a member of the membrane associated guanylate kinases localised to intercellular contacts.[28] ZO-1 binds various proteins, including claudins and occludin, and may act as a molecular scaffold bringing these TJ constituents together.[29] Therefore, ZO-1 is expected to be a key molecule in the control of BNB integrity,

despite some previous conclusions that the expression and localisation of ZO-1 do not correlate with the physiological efficiency of paracellular barrier function.[30] In CIDP specimens, we found no significant decrease in ZO-1 immunoreactive endoneurial microvessels, although we noted a change in the staining pattern. This corresponds well with a recent observation that VEGF, known to open the BBB and BNB,[14] caused a loss of ZO-1 from endothelial cell junctions and changed the staining pattern at the cell boundary without decreasing ZO-1 content in cultured bovine BMEC.[27] We suspect that the change in the localisation of ZO-1 in CIDP specimens was an effect of various cytokines, including VEGF, that are upregulated in inflammatory neuropathies such as CIDP. The contribution of other inflammatory cytokines in addition to VEGF requires future investigation.

Authors' affiliations
T Kanda, Y Numata, H Mizusawa, Department of Neurology and Neurological Science, Tokyo Medical and Dental University Graduate School, 1-5-45 Yushima, Bunkyo-ku, Tokyo 113-8519, Japan

Competing interest: none declared

REFERENCES

1 **Reese TJ,** Karnovsky MJ. Fine structural localization of a blood–brain barrier to exogenous peroxidases. *J Cell Biol* 1967;**34**:207–17.
2 **Rubin LL.** Endothelial cells: adhesion and tight junction. *Curr Opin Cell Biol* 1992;**4**:830–3.
3 **Kanda T,** Yamawaki M, Mizusawa H. Sera from Guillain-Barré patients enhance leakage in blood–nerve barrier model. *Neurology* 2003;**60**:301–6.
4 **Furuse M,** Hirase T, Itoh M, *et al.* Occludin: a novel integral membrane protein localizing at tight junctions. *J Cell Biol* 1993;**123**:1777–88.
5 **Hirase T,** Staddon JM, Saitou M, *et al.* Occludin as a possible determinant of tight junction permeability in endothelial cells. *J Cell Sci* 1997;**110**:1603–13.
6 **Saitou M,** Fujimoto K, Doi Y, *et al.* Occludin-deficient embryonic stem cells can differentiate into polarized epithelial cells bearing tight junctions. *J Cell Biol* 1998;**141**:397–408.
7 **Furuse M,** Fujita K, Hiiragi T, *et al.* Claudin-1 and -2: novel integral membrane proteins localizing at tight junctions with no sequence similarity to occludin. *J Cell Biol* 1998;**141**.1539–50.
8 **Morita K,** Furuse M, Fujimoto K, *et al.* Claudin multigene family encoding four-transmembrane domain protein components of tight junction strands. *Proc Natl Acad Sci U S A* 1999;**96**:511–16.
9 **Morita K,** Sasaki H, Fujimoto K, *et al.* Claudin-11/OSP-based tight junctions of myelin sheaths in brain and Sertoli cells in testis. *J Cell Biol* 1999;**145**:579–88.
10 Research criteria for diagnosis of chronic inflammatory demyelinating polyneuropathy (CIDP). Report from an ad hoc subcommittee of the American Academy of Neurology AIDS Task Force. *Neurology* 1991;**32**:958–64.
11 **Sharief MK,** Ingram DA, Swash M. Circulating tumor necrosis factor-alpha correlates with electrodiagnostic abnormalities in Guillain-Barré syndrome. *Ann Neurol* 1997;**42**:68–73.
12 **Zhu J,** Bai XF, Mix E, *et al.* Experimental allergic neuritis: cytolysin mRNA expression is upregulated in lymph node cells during convalescence. *J Neuroimmunol* 1997;**78**:108–16.
13 **Watanabe O,** Arimura K, Kitajima I, *et al.* Greatly raised vascular endothelial growth factor (VEGF) in POEMS syndrome. *Lancet* 1996;**347**:702.
14 **Kanda T,** Iwasaki T, Yamawaki M, *et al.* Anti-GM1 antibody facilitates leakage in an in vitro blood–nerve barrier model. *Neurology* 2000;**55**:585–7.
15 **Gale NW,** Yancopoulos GD. Growth factors acting via endothelial cell-specific receptor tyrosine kinases: VEGFs, angiopoietins, and ephrins in vascular development. *Genes Dev* 1999;**13**:1055–66.
16 **Kevil CG,** Payne DK, Mire E, *et al.* Vascular permeability factor/vascular endothelial cell growth factor-mediated permeability occurs through disorganization of endothelial junctional proteins. *J Biol Chem* 1998;**273**:15099–103.
17 **Tsukita S,** Furuse M. Pores in the wall: claudins constitute tight junction strands containing aqueous pores. *J Cell Biol* 2000;**149**:13–16.
18 **Gow A,** Southwood CM, Li JS, *et al.* CNS myelin and Sertoli cell tight junction strands are absent in Osp/claudin-11 null mice. *Cell* 1999;**99**:649–59.
19 **Simon DB,** Lu Y, Choate KA, *et al.* Paracellin-1, a renal tight junction protein required for paracellular Mg^{2+} resorption. *Science* 1999;**285**:103–6.
20 **Morita K,** Sasaki H, Furuse M, *et al.* Endothelial claudin: claudin-5/TMVCF constitutes tight junction strands in endothelial cells. *J Cell Biol* 1999;**147**:185–94.
21 **Nitta T,** Hata M, Gotoh S, *et al.* Size-selective loosening of the blood–brain barrier in claudin-5 deficient mice. *J Cell Biol* 2003;**161**:653–60.
22 **Kanda T,** Yamawaki M, Iwasaki T, *et al.* Glycosphingolipid antibodies and blood–nerve barrier in autoimmune demyelinative neuropathy. *Neurology* 2000;**54**:1459–64.
23 **Lewis RA,** Sumner AJ. Electrophysiologic features of inherited demyelinating neuropathies: a reappraisal. *Ann N Y Acad Sci* 1999;**883**:321–5.
24 **Bell MA,** Weddell AGM. A descriptive study of the blood vessels of the sciatic nerve in the rat, man, and other mammals. *Brain* 1984;**107**:871–98.
25 **Latker CH,** Wadhwani KC, Baldo A, *et al.* Blood–nerve barrier in the frog during Wallerian degeneration: are axons necessary for maintenance of barrier function? *J Comp Neurol* 1991;**309**:650–64.
26 **Saitou M,** Ando-Akatsuka Y, Itoh M, *et al.* Mammalian occludin in epithelial cells: its expression and subcellular distribution. *Eur J Cell Biol* 1997;**73**:222–31.
27 **Wang W,** Dentler WL, Borchardt RT. VEGF increases BMEC monolayer permeability by affecting occludin expression and tight junction assembly. *Am J Physiol* 2001;**280**:H434–40.
28 **Mitic LL,** Anderson JM. Molecular architecture of tight junctions. *Annu Rev Physiol* 1998;**60**:121–42.
29 **Zahraoui A,** Louvard D, Galli T. Tight junction, a platform for trafficking and signaling protein complexes. *J Cell Biol* 2000;**151**:F31–6.
30 **Stevenson BR,** Anderson JM, Goodenough DA, *et al.* Tight junction structure and ZO-1 content are identical in two strains of Madin-Darby canine kidney cells which differ in transepithelial resistance. *J Cell Biol* 1988;**107**:2401–8.

Journal of Neuroscience Research 78:141–150 (2004)

Glycosphingolipid Composition of Primary Cultured Human Brain Microvascular Endothelial Cells

Takashi Kanda,[1]* Toshio Ariga,[2] Hisako Kubodera,[1] Hong Lian Jin,[1] Kiyoshi Owada,[1] Takeshi Kasama,[3] Masanaga Yamawaki,[1] and Hidehiro Mizusawa[1]

[1]Department of Neurology and Neurological Science, Tokyo Medical and Dental University Graduate School, Tokyo, Japan

[2]Drug Development Technology, Eisai Co. Ltd., Tokyo, Japan

[3]Instrumental Analysis Research Center of Life Science, Tokyo Medical and Dental University Graduate School, Tokyo, Japan

Glycosphingolipid (GSL) antigens have been considered to be involved in the pathogenesis of autoimmune neurologic disorders including multiple sclerosis. To establish the GSL pattern specific for endothelial cells forming blood–brain barrier (BBB), we established a method to yield sufficient quantities of highly purified human brain microvascular endothelial cells (HBMECs) and compared their GSL composition to that of human umbilical cord vein endothelial cells (HUVECs), as the representative of endothelial cells not forming BBB. The major gangliosides were GM3 and sialyl paragloboside (LM1), and the major neutral GSLs were lactosylceramide (LacCer), globotriaosylceramide (Gb3), and globoside (Gb4). Trace amounts of GM1, GD1a, GD1b, GT1b, and sulfoglucuronosyl paragloboside (SGPG) could be detected by the high performance thin layer chromatography-overlay method. SGPG was detected only at a nonconfluent state in an amount almost 1/30 that of in nonconfluent HUVECs. Conversely, GM3 and LM1 increased significantly after confluency. The amount of Gb3 in HBMECs was almost as twice that in HUVECs. The significance of these differences in GSL content between HBMECs and HUVECs and between confluent and nonconfluent states is obscure. It might be related, however, to the defense mechanism at the BBB and to the susceptibility of the central nervous system in some disorders that target cell surface GSL, such as hemolytic uremic syndrome.

Key words: glycosphingolipid; sulfoglucuronosyl paragloboside; blood–brain barrier; human brain microvascular endothelial cell

Vascular endothelial cells (ECs) are highly versatile cells and are involved structurally as well as metabolically in various barrier functions. The characteristic features of ECs include the presence of nonthrombogenic luminal surface, expression of von Willebrand factor, prostacycline, and endothelin, and formation of a highly selective barrier to the passage of plasma constituents into the tissue parenchyma. ECs possess many structural and functional characteristics, exhibiting a wide diversity depending on the nature of the vascular bed; this property is very important for their specialized function in individual tissue and organ function (Jaffe, 1987; Kanda et al., 1994). ECs of brain microvascular origin (BMECs) are highly specialized cells believed to make up the structural basis of the blood–brain barrier (BBB). Because BMECs are the only cell groups in the nervous system that are exposed continuously to blood constituents, the information via surface receptors on BMECs are considered very important for regulation of BBB function and subsequently for homeostasis of various cations, nutrients, and growth factors in the central nervous system (CNS).

Glycosphingolipids (GSLs) are located primarily, if not exclusively, on the outer leaflet of the plasma mem-

Abbreviations: BBB, blood–brain barrier; BMEC, brain microvascular endothelial cell; BNB, blood–nerve barrier; CNS, central nervous system; DiI-Ac-LDL, 1, 1′-dioctacecyl-3,3,3′,3, tetramethyl indocarbocyanine perchlorate acetylated low-density lipoprotein; DM, Dissecting medium; EC, endothelial cell; Gb3, globotriaosylceramide; Gb4, globoside; GSL, glycosphingolipid; HBMEC, human brain microvascular endothelial cell; HPTLC, high-performance thin-layer chromatography; HUS, hemolytic uremic syndrome; HUVEC, human umbilical cord vein endothelial cell; LM1, sialyl paragloboside; LacCer, lactosylceramide; *mdr1*, multidrug resistance-1 gene; PBS, phosphate buffered-saline; PnMEC, microvascular endothelial cell of endoneurial tissue origin; PNS, peripheral nervous system; SGPG, sulfoglucuronosyl paragloboside; SIMS, matrix-assisted secondary ion mass spectrometry.

Contract grant sponsor: Ministry of Education, Science, and Culture of Japan.

*Correspondence to: Dr. Takashi Kanda, Department of Neurology and Neurological Science, Tokyo Medical and Dental University Graduate School, 1-5-45, Yushima, Bunkyo-ku, Tokyo 113-8519, Japan.
E-mail: t-kanda.nuro@tmd.ac.jp

Received 12 February 2004; Revised 25 May 2004; Accepted 1 June 2004

Published online 23 August 2004 in Wiley InterScience (www.interscience.wiley.com). DOI: 10.1002/jnr.20228

brane. GSLs, including gangliosides, have been implicated in various cellular functions such as cellular recognition and adhesion, communication, and modulation of immune responses (Kanda et al., 1995; Karlsson, 1995; Riboni et al., 1997). Knowledge about GSLs as surface antigens and receptors in BMECs is therefore crucial to understanding the pathogenesis of CNS disorders affecting the BBB. Because of the difficulty in primary culture and the maintenance of human BMECs (HBMECs), however, no data concerning the GSL composition in these cells has ever been published. Duvar et al. (2000) recently investigated the GSL composition of immortalized human cerebromicrovascular endothelial cells; however, because this endothelial cell line cannot exclude the influence of immortalization with SV40 T-antigen, GSL analysis of genuine primary cultured HBMECs has been awaited eagerly.

We recently developed a method to yield sufficient quantities of highly purified HBMECs for biochemical analysis, and we have determined the GSL composition of cultured HBMECs. The aim of this article is to establish the GSL pattern specific for the ECs forming BBB, compared to that of human umbilical cord vein endothelial cells (HUVECs) as the representative of ECs without BBB property.

MATERIALS AND METHODS

Culture Media for HBMECs

Dissecting medium (DM) contained Medium 199 (GIBCO BRL, Grand Island, NY) supplemented with 5% fetal bovine serum (FBS; BioWhittaker, Walkersville, MD), 20 mM sodium bicarbonate, 50 μg/ml heparin (Sigma, St. Louis, MO), 100 U/ml penicillin, 100 μg/ml streptomycin, 25 ng/ml amphotericin B (GIBCO BRL), and 20 mM *N*-(2-hydroxymethyl)-piperazine-*N'*-(2-ethanesulfonic acid) (HEPES; pH 7.2). HBMEC growth medium contained EBM-2 media (Sanko Jun-yaku, Tokyo, Japan) supplemented with 100 U/ml penicillin, 100 μg/ml streptomycin, and 25 ng/ml amphotericin B.

Isolation of HBMECs

HBMEC isolation was achieved using a modified method of Gordon et al. (1991), which was designed originally for rat capillary endothelial cells. Brain tissue was removed approximately 6 hr postmortem from a 65-year-old male who had suffered from lung cancer. The tissue was rinsed thrice with DM, and the pia mater and surface vessels were removed carefully using fine forceps. The cerebral cortex was then minced to 2–3-mm cubes, rinsed several times in DM, and homogenized using a Wheaton-Dounce Teflon homogenizer. The homogenate was dissociated further with 0.005% (wt/vol) dispase (grade 1; Roche Diagnostics, Mannheim, Germany) in DM at 37°C for 2 hr in a shaking water bath. After centrifugation (800 × *g*, 5 min) the pellet was suspended with a dextran solution (mol. wt. 70,000 Daltons; 15% wt/vol in DM; Sigma), and the whole suspension was centrifuged (4°C, 4,500 × *g* for 10 min, using a Beckman JS 13.1 swinging bucket rotor). The pellet was resuspended with the dextran solution, and centrifuged again. After two centrifugations, microvessels and some single cells including red blood cells were obtained in the pellet. Other contaminating fractions including myelin and brain parenchyma were floated. The pellet was recovered with DM and filtered through 130-μm nylon mesh (Nitex; Tetko Inc., Elmsford, NY) to remove large vessels. The filtrate was digested further using collagenase/dispase (0.035% wt/vol in 10 ml DM; Roche Diagnostics) at 37°C for 12 hr in a shaking water bath. The collagenase/dispase-treated microvessels were centrifuged (800 × *g*, 5 min), rinsed and suspended in 3.0 ml DM, and then filtered through double layers of 15-μm mesh to remove single cells, which were the largest sources of non-ECs, including astrocytes and pericytes. The unfiltered cell clusters were placed into dishes coated with type I collagen (Collaborative Biomedical Products, Bedford, MA). Cells were maintained at 37°C in an atmosphere of 5% CO_2 in a humidified incubator. The medium was changed three times a week.

After 24 hr, the first migrated ECs were observed from the edge of seeded cell clusters. When the EC colonies grew sufficiently large for cloning (usually more than 100 ECs), the medium was replaced by 0.25% pancreatin solution (GIBCO BRL). The colonies for cloning (free of contamination of non-ECs, including pericytes) were marked before pancreatin treatment. The colonies were detached as clumps of ECs, and the marked colonies were picked up using a Pasteur pipette and were dissociated briefly in 0.1% trypsin in Ca^{2+}, Mg^{2+}-free Hanks' solution for 3–4 min. Cells were seeded again on 35-mm Petri dishes coated with type I rat tail collagen. After 10–21 days, confluent HBMECs, almost free of contaminating non-ECs, were subcultured at a split ratio of 1:3–5.

Identification of HBMECs

HBMECs were identified by the following four criteria: an elongated cobblestone-like appearance; immunoreactivity to anti-von Willebrand factor antigen antibody; uptake of 1, 1'-dioctacecyl-3,3,3',3, tetramethyl indocarbocyanine perchlorate acetylated low-density lipoprotein (DiI-Ac-LDL; Biomedical Technologies Inc., Stoughton, MA) (Voyta et al., 1984); and the expression of the multidrug resistance-1 (*mdr1*) gene. To label with DiI-Ac-LDL, cells were incubated with 10 μg/ml of DiI-Ac-LDL at 37°C in HBMEC growth media for 4 hr. Cells were then washed once with probe-free media for 10 min, fixed with 4% paraformaldehyde for 30 min, and viewed under a fluorescent microscope. HBMECs incorporated the bright DiI-Ac-LDL particles into their cytoplasm. Only the lots of HBMECs with more than 98% of DiI-Ac-LDL-positive cells were used for further analysis. Contaminated cells other than endothelial cells were also evaluated using mouse anti-human antibodies against glial fibrillary acidic protein (GFAP; Sigma), α smooth muscle actin (BioGenex Laboratories, San Ramon, CA), and galactocerebroside (Sigma). Less than 1% of cells were immunoreactive with these antibodies. Expression of *mdr1* mRNA, one of the most reliable pieces of evidence of their BBB-forming endothelial cell origin, was confirmed using Takara Human 3K Chip v.3.0 (Takara, Tokyo, Japan). Absence of *mdr1* mRNA in HUVEC was also confirmed.

Isolation of Glycosphingolipids

Cultured HBMECs and HUVECs (purchased from Sanko Jun-Yaku), grown confluently or semiconfluently on 100-mm Petri dishes, were harvested by scraping from the Petri dishes,

TABLE I. Glycosphingolipid Composition of Cultured HBMECs and HUVECs†

Glycosphingolipid	HBMEC-C	HBMEC-NC	HUVEC-C	HUVEC-NC
Acidic				
GM3	1,226 ± 321	254 ± 110*	2,321 ± 166	1,226 ± 194
LM1	583 ± 103	178 ± 36**	879 ± 314	464 ± 81
GM1	7.1 ± 0.9	6.2 ± 1.6	8.5 ± 1.7	6.0 ± 0.5
GD1a	4.3 ± 0.6	3.7 ± 1.0	3.0 ± 0.9	2.6 ± 0.7
GD1b	Trace	Trace	Trace	Trace
GT1b	2.5 ± 1.0	2.7 ± 0.9	2.5 ± 0.5	1.8 ± 0.9
Neutral				
LacCer	295 ± 102	182 ± 88	368 ± 139	339 ± 54
Gb3	548 ± 131	612 ± 185	259 ± 66	269 ± 62
Gb4	1,852 ± 483	1,359 ± 383	1,195 ± 530	1,205 ± 304

†HBMEC-C, human brain microvascular endothelial cell, confluent state; HBMEC-NC, human brain microvascular endothelial cell, nonconfluent state; HUVEC-C, human umbilical cord vein endothelial cell, confluent state; HUVEC-NC, human umbilical cord vein endothelial cell, nonconfluent state. Values were expressed as ng ± SEM per mg protein; $n = 3$.
*$P < 0.05$ vs. HBMEC-C and $P < 0.01$ vs. HUVEC-C.
**$P < 0.01$ vs. HBMEC-C and $P < 0.05$ vs. HUVEC-C.

washed two times with PBS, pH 7.3, and homogenized in 0.5 ml of distilled water. *Nonconfluent* or *semiconfluent* culture denotes the condition where endothelial cell-free vacant space, more than 20% of total culture dish surface, is visible under inverted microscopy. These cells are expected to be still proliferating. *Confluent* culture denotes that the endothelial cells are tightly packed and no cell-free vacant space is recognizable under inverted microscopy. Cells within the fourth passage were used for GSL analysis. Protein concentrations were determined according to the method of Bradford (1976) using a Bio-Rad (Richmond, CA) protein assay kit and bovine serum albumin (BSA) as standard. Lipids were extracted with 5 ml of chloroform/methanol (1:1 by volume), and 5 ml of chloroform/methanol (1:2 by volume), successively. After evaporating the organic solvents under a nitrogen stream, lipids were dissolved in 0.5 ml chloroform/methanol/water (30:60:8 by volume; solvent A), and applied to a Sephadex LH-20 column (0.5 × 30 cm, 10-ml bed volume; Pharmacia Fine Chemicals), pre-equilibrated with solvent A. After the first 3 ml of effluent was discarded, the next 3 ml was collected as a GSL fraction (Yu et al., 1994). The GSL fraction was then applied to a DEAE-Sephadex A-25 column (2.0-ml bed volume; Pharmacia Fine Chemicals). The neutral GSL fraction was eluted with 20 ml of solvent A, and the acidic GSL fraction was eluted with 20 ml of chloroform/methanol/0.8 M sodium acetate (30:60:8 by volume; solvent B) (Yu et al., 1994). The acidic lipid fraction was evaporated to dryness and the residue was dissolved in 0.5 ml of solvent A, and then desalted by Sephadex LH-20 column as described above. The recovered gangliosides and sulfoglucuronosyl paragloboside (SGPG) were developed on a high-performance thin-layer chromatographic plate (HPTLC; Merck, Darmstadt, Germany) with the solvent system of chloroform/methanol/water containing 0.22% $CaCl_2 \cdot 2H_2O$ (55:45:10 by volume; solvent system I) and the bands were visualized by spraying the plate with resorcinol-HCl (Ando et al., 1978; Sekine et al., 1984).

The neutral GSL fraction was evaporated to dryness and the residue was subjected to mild alkaline treatment (0.5 ml of 0.4 N NaOH in methanol) at 40°C for 2 hr or room temperature overnight to remove phospholipids according to the method of Handa (1963). The reaction mixtures were applied to a Sephadex LH-20 column to remove salts as described above. Neutral GSL composition was examined by HPTLC. Before chromatography, the upper half of the plate was sprayed with 1% borate and the entire plate was activated for 30 min at 120°C to detect glucosyl ceramide and galactosyl ceramide. After application of the sample, the plate was developed with a solvent system of chloroform/methanol/water (65:35:5 by volume, solvent system II). Neutral GSLs were visualized by spraying with the orcinol-sulfuric acid reagent. The nomenclature of gangliosides follows the system of Svennerholm (1964).

Quantitation of GM3 (NeuAc), Sialyl Paragloboside (NeuAc-nLcOse$_4$), and Other Ganglio-*N*-Tetraosyl Gangliosides

The content of GM3 (NeuAc) and sialyl paragloboside (LM1) was determined by densitometric scanning of the chromatographic plate with comigration of authentic GM3 (NeuAc) and LM1, followed by visualizing with the resorcinol-HCl reagent (Ando et al., 1978). The structure of LM1 was confirmed immunochemically with the HPTLC-overlay method using anti-paragloboside (nLcOse$_4$) monoclonal antibody (kindly provided by Dr. Tai) after treatment with *Arthrobacter ureafaciens* neuraminidase (40 mU/ml) for 2 hr at room temperature. The amounts of ganglio-*N*-tetraosyl gangliosides other than GM3 were below the detection limit of the resorcinol-HCl reagent. The HPTLC plate was therefore developed with solvent system I and bands were incubated with *A. ureafaciens* neuraminidase (40 mU/ml) for 2 hr at room temperature and then overlaid with anti-rabbit asialo GM1 antibody (diluted 1:25) for 2 hr to detect these minor ganglio-*N*-tetraosyl species (Saito et al., 1985).

Quantitation of Neutral GSLs

The presence of Gb3 and Gb4 was confirmed using anti-Gb3 and anti-Gb4 monoclonal antibodies (kindly provided

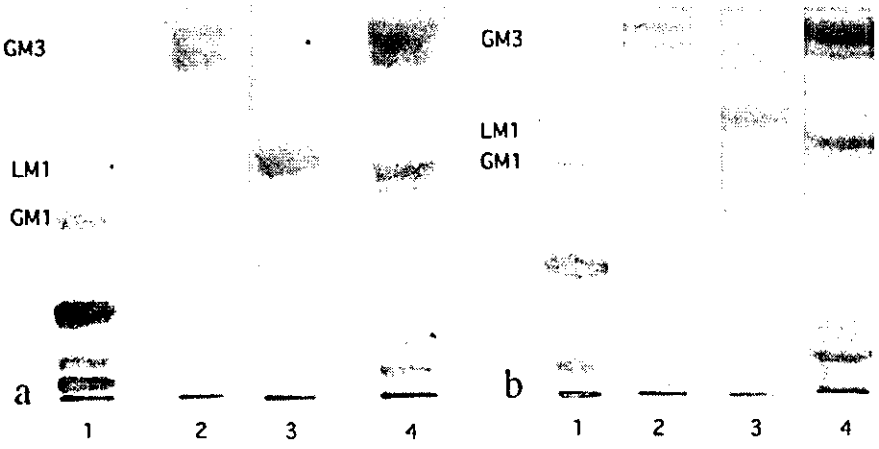

Fig. 1. Acidic glycosphingolipid (GSL) fraction in HUVECs (a) and HBMEC (b). Lane 1, human brain ganglioside standards (5 μg); lane 2, 1 μg of standard GM3 (NeuAc); lane 3, 1 μg of standard LM1; lane 4, acidic GSL fraction obtained from HUVECs (a) and HBMECs (b). The bands were visualized with the resorcinol-HCl reagent.

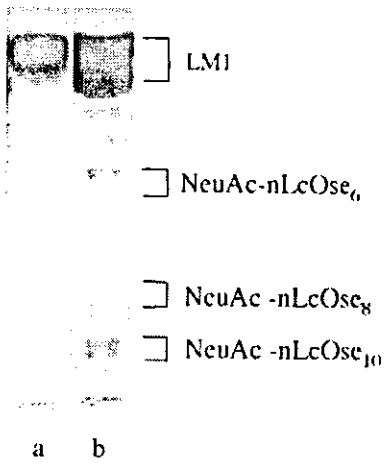

Fig. 2. **a:** Standard LM1 (1 μg). **b:** HPTLC-overlay method of acidic GSL fraction in HBMECs with the anti- nLcOse$_4$ monoclonal antibody after treatment with *A. ureafaciens* neuraminidase.

by Dr. Tai). The content of LacCer, Gb3, and Gb4 was determined by densitometric scanning of the chromatographic plate with comigration of authentic LacCer, Gb3, and Gb4, followed by visualizing with orcinol-sulfuric acid reagent.

Quantitation of SGPG (HPTLC-Overlay Method With Anti-SGPG Antibody)

Quantitative analysis of SGPG was achieved by the method described previously (Kanda et al., 1994). After the GSL fraction (collected from approximately 8–20-mg protein sample) and authentic SGPG (from 2–120 ng in quantity) were chromatographed in solvent system I, the plate was dipped in 0.4% polyisobutylmethacrylate solution in hexane for 1 min and air-dried. The plate was then incubated with LT serum (anti-SGPG antibody; immunoglobulin [Ig]M) for 2 hr, the serum from a patient with demyelinative neuropathy and IgM paraproteinemia that recognizes HNK-1 epitope, at a dilution of 1:1,000 in dilution buffer, followed by peroxidase conjugated rabbit anti-human IgM (μ-chain specific, 1:1,000; Cappel) for 2 hr. The LT serum (anti-SGPG antibody) was a generous gift from Dr. R.K. Yu (Department of Biochemistry and Molecular Biology, Institute of Molecular Medicine and Genetics, Medical College of Georgia, Augusta, GA). After washing with PBS, the plate was visualized with a Konica Immunostaining HRP 1000 (Konica, Seikagaku-kogyo, Japan). Although LT serum can react with SGPG, sulfoglucuronosyl lactosaminyl paragloboside (SGLPG) and band X (Ariga et al., 1987), only SGPG could be detected in HBMECs and HUVECs. SGPG was quantitated based on standard curves generated by densitometric scanning of known amounts of SGPG developed on the same plate.

Immunostaining of HBMECs and HUVECs With Anti-SGPG Antibody

Confluently or nonconfluently cultured HBMECs and HUVECs on collagen type I-coated glass slides were fixed with 4% paraformaldehyde for 15 min and washed with PBS at least three times. After incubation in PBS with 3% nonimmunized rabbit serum, LT serum (anti-SGPG antibody; diluted 1:100 in PBS) was applied at 4°C for 72 hr. The slides were washed three times and fluorescein isothiocyanate (FITC)-conjugated rabbit anti-human IgM (μ-chain specific, 1:1,000; Cappel) was applied for 1 hr at room temperature.

HPTLC/Matrix-Assisted Secondary Ion Mass Spectrometry

Negative secondary ion mass spectrometry (SIMS) spectra of GSLs were recorded on a Finnigan TSQ 70 quadrupole mass spectrometer in the negative ion mode equipped with a cesium ion (Cs) gun as follows. After developing GSLs on an HPTLC plate, a primuline reagent was sprayed over the plate until it is visibly wet GSLs on the plate were viewed under UV light at 380 nm. Each GSL band was marked with a colored drawing pencil while still under illumination. The plate was then immersed for 20 sec in a solvent composed of 2-propanol:methanol:0.2% aqueous $CaCl_2$ (40:20:7, vol/vol). It was then placed on another glass plate, after which a polyvinylidene difluoride (PVDF) membrane sheet and a glass microfilter sheet were

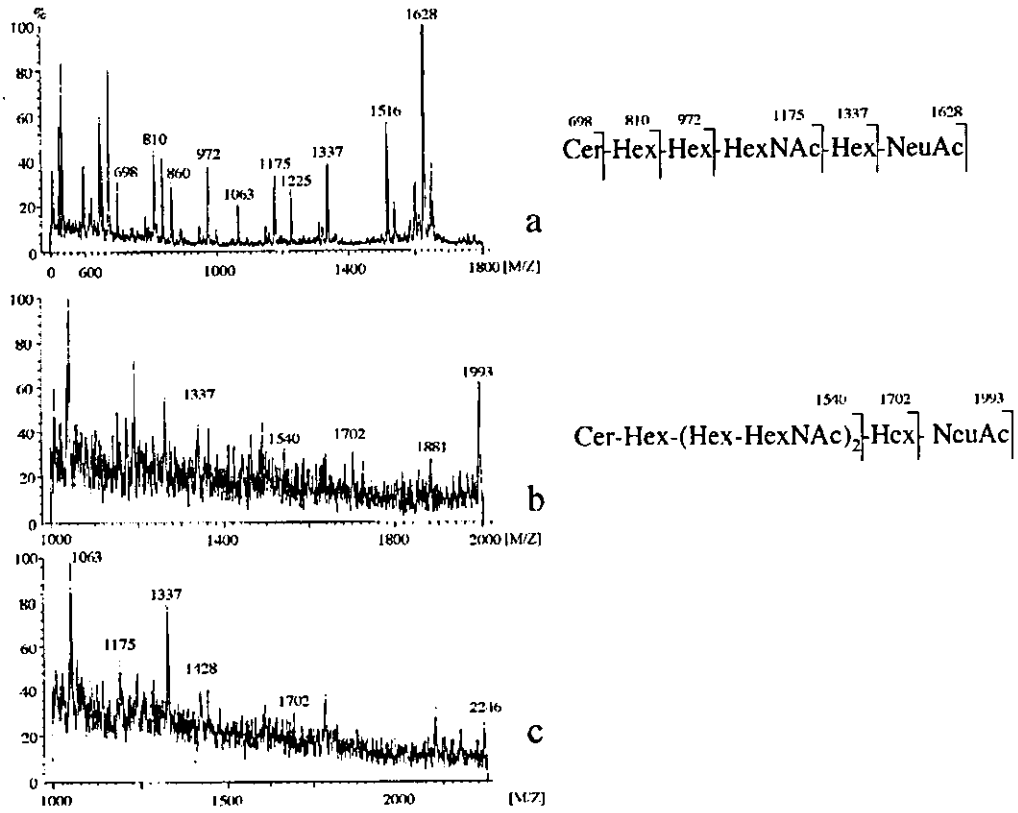

Fig. 3. Mass spectrometry of LM1 (a), NeuAc-nLcOse$_6$ (b), and NeuAc-nLcOse$_8$ (c) from HBMECs.

placed over the plate. The "sandwich" was then pressed with a household iron (about 180°C) for 30 sec. The PVDF membrane was separated from the HPTLC plate, washed with water to remove the primuline reagent, and then dried. The GSL band on the PVDF membrane was excised (2 mm in diameter) and placed on a mass spectrometer prove tip, and few microliters of triethanolamine was added as the matrix. Samples on the membrane were bombarded with a Cs^+ beam at 20 kV. The ion multiplier was kept at 1.5 kV and the conversion dynode at 20 kV (Ishikawa et al., 1995; Taki et al., 1995).

RESULTS

Glycosphingolipid composition of cultured HBMECs and HUVECs are shown in Table I.

Ganglioside Composition in HBMECs

Figure 1 shows the ganglioside pattern of the HBMECs. The two major gangliosides were identified as GM3 (NeuAc) and sialyl paragloboside (LM1; NeuAc-nLcOse$_4$) using authentic samples of GM3 (NeuAc) and LM1. LM1 was identified by HPTLC-overlay method using anti-paragloboside monoclonal antibody after neuraminidase treatment (see Fig. 2). Most bands observed in polysialoganglioside regions (Fig. 1a,b; lane 4) are neolacto-*N*-tetraose series gangliosides; it was impossible to detect ganglio-*N*-tetraose series gangliosides using resorcinol-sulfuric acid reagent (Kanda et al., 1994). In addition, this method revealed that acidic GSL fraction contained several gangliosides containing paragloboside core structures (lacto-*N*-tetraose series gangliosides; Fig. 2). The structures of these gangliosides were confirmed by HPTLC/matrix-assisted SIMS (Ishikawa et al., 1995; Taki et al., 1995) as shown in Figure 3. Negative SIMS mass spectra of gangliosides can provide information on their molecular weights and sugar sequences as well as their fatty acid and long chain base compositions. The mass spectra revealed prominent deprotonated molecules $[M - H]^-$, which corresponded to GSL molecular species containing fatty acids with chain lengths ranging from C18:0 to C24:0 and C18 sphingenine. The band comigrating to LM1 was ceramide (Cer) pentasaccharide that was found to be Cer (m/e 536-m/z 648), Cer-Hex (m/z 698-m/z 810), Cer-Hex-Hex (m/z 860-m/z 972), Cer-Hex-Hex-HexNAc (m/z 1063-m/z 1175), Cer-Hex-Hex-HexNAc-Hex (m/z 1225-m/z 1337) and Cer-Hex-Hex-HexNAc-Hex-NeuAc ($[M - H]^-$; m/z 1517-m/z 1629) (Fig. 3a). The lower band of LM1 that reacted with

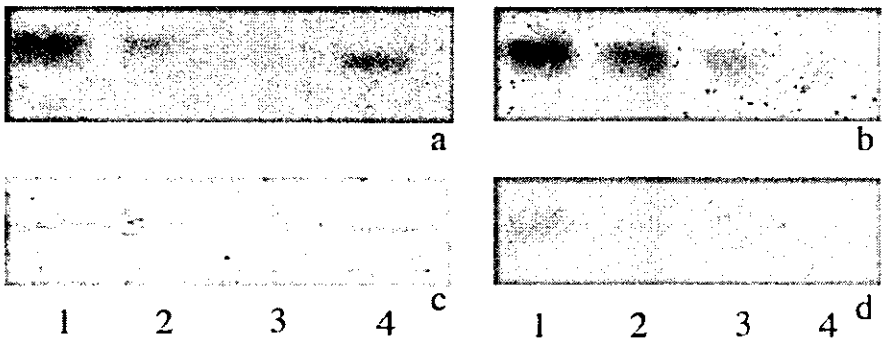

Fig. 4. HPTLC-overlay method of SGPG at a nonconfluent state in HUVECs (a) and HBMECs (c) and after confluency in HUVECs (b) and HBMECs (d). Lanes 1–3: 1.6, 0.8, and 0.4 ng of standard SGPG, respectively. Lane 4: in (a), acidic GSL fraction from 0.05 mg protein of HUVECs at nonconfluent state; in (b), acidic GSL fraction from 0.5 mg protein of HUVECs after confluency; in (c), acidic GSL fraction from 1 mg protein of HBMECs at a nonconfluent state; and in (d), acidic GSL fraction from 1 mg protein in HBMECs after confluency.

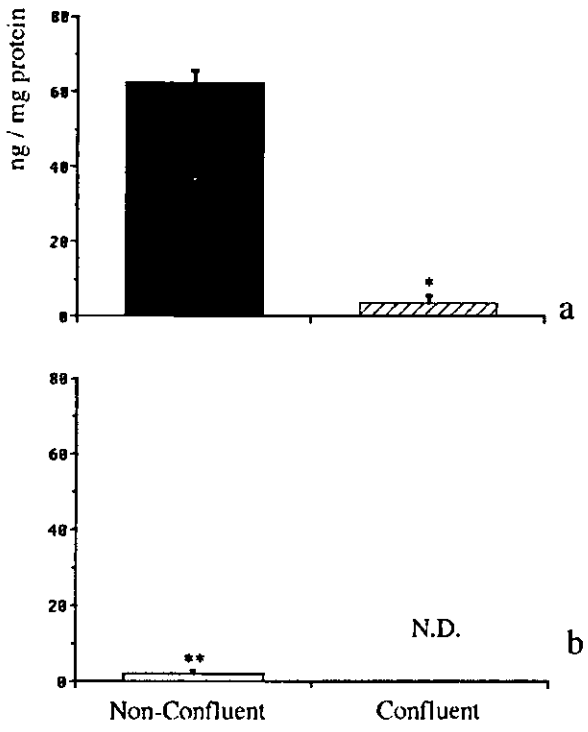

Fig. 5. SGPG content in HUVECs (a) and HBMECs (b) at nonconfluent state and after confluency. $n = 3$. Bars denote SEM. $*P < 0.0001$; $**P < 0.001$ vs. HUVECs at a nonconfluent state (black bar).

anti-paragloboside monoclonal antibody showed the deprotonated molecules (m/z 1516-m/z 1628), suggesting the presence of positional isomer of LM1 containing NeuAc (2→6) (data not shown), which the structure of NeuAc (2→6)-nLcOse$_4$ was reported by several investigators (Fukuda et al., 1985; Nojiri et al., 1988). The band that migrated to the middle position was Cer-heptasaccharide, which was found to be Cer-Hex-Hex-HexNAc-Hex (m/z 1225-m/z 1337), Cer-Hex-Hex-HexNAc-Hex-HexNAc (m/z 1428-m/z 1540), Cer-Hex-Hex-HexNAc-Hex-HexNAc-Hex (m/z 1590-m/z 1702), and Cer-Hex-Hex-HexNAc-Hex-HexNAc-Hex-NeuAc ($[M - H]^-$; m/z 1881-m/z 1993) (Fig. 3b). The second band migrated from the bottom was supposed to be Cer-nonasaccharide, but was found to be Cer-Hex-Hex-HexNAc-Hex (m/z 1225-m/z 1337), Cer-Hex-Hex-HexNAx-Hex-HexNAc (m/z 1428), Cer-Hex-Hex-HexNAc-Hex-HexNAc-Hex (m/z 1702), and Cer-Hex-Hex-HexNAc-Hex-HexNAc-Hex-HexNAc-Hex-NeuAc ($[M - H]^-$; m/z 2246) containing C18:0 fatty acid and sphingenine. Unfortunately, the deprotonated molecule at m/z 2359 containing C24:0 fatty acid and sphingenine was not detected because it was out of scales. The lower band reacted with anti-paragloboside monoclonal antibody may be ceramide containing 11 saccharides because several ions containing background ions were detected in near the deprotonated molecules (m/z 2612 - m/z 2724; data not shown). In HBMECs, GM3 and LM1 increased significantly after confluency ($P < 0.05$ and $P < 0.01$, respectively). Four ganglio-*N*-tetraosyl gangliosides, including GM1, GD1a, GD1b, and GT1b, were also detected in HUVECs and HBMECs as minor species using *A. ureafaciens* neuraminidase and anti-asialo GM1 antibody (Saito et al., 1985). No appreciable difference was noted, however, in their compositions before and after confluency.

SGPG in HBMECs and HUVECs

SGPG was found in the GSL fraction of HBMECs and HUVECs by the HPTLC-immunostaining method (Fig. 4). Neither SGLPG nor band X, found previously in human peripheral nerve (Kohriyama et al., 1987), could be detected by this method. The latter was identified as

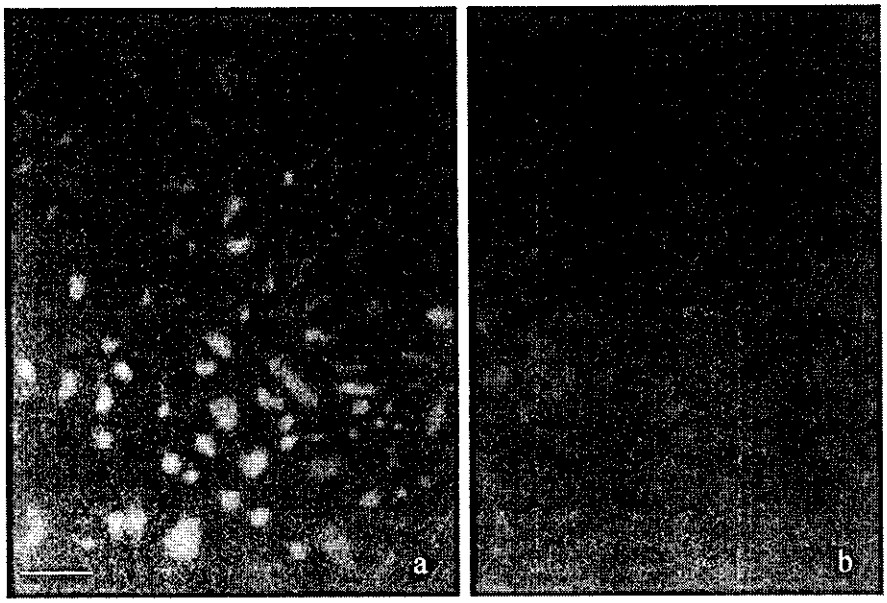

Fig. 6. Immunostaining of HUVECs before (a) and after (b) confluency using LT serum (anti-SGPG antibody). In HBMECs, no appreciable immunofluorescence was detected (data not shown). Scale bar = 100 μm.

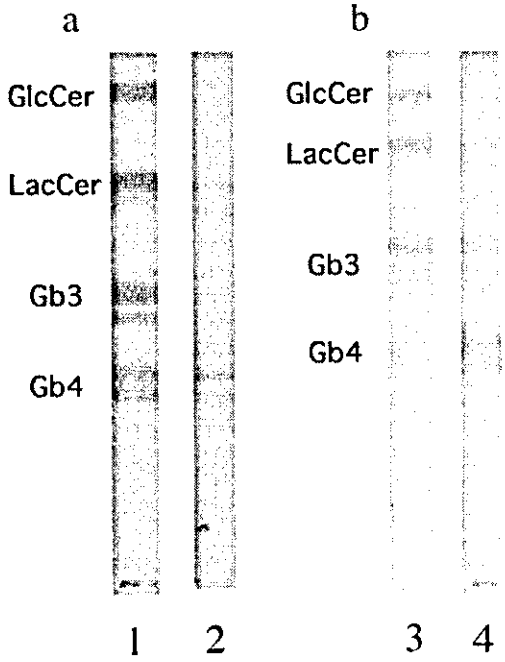

Fig. 7. Thin-layer chromatogram of neutral GSLs in HUVEC (a) and HBMEC (b). Lanes 1 and 3: 1 μg each of authentic GlcCer from human brain, LacCer, Gb3, Gb4 from porcine erythrocyte membranes (from top to bottom). Lane 2: neutral GSL fraction from HUVECs. Lane 4: neutral GSL fraction from HBMECs.

lysophosphatidylinositol (Suzuki et al., 2001). Figure 5 shows the quantitative difference of SGPG in HBMECs and HUVECs, at confluent as well as at nonconfluent culture phases. Under the nonconfluent condition, especially, when endothelial cells are in the proliferation phase and cell-to-cell contact is not conspicuous, the SGPG content in HUVECs was more than forty times as abundant as that in HBMECs. After confluency, the SGPG content in HUVECs was decreased (1/30) and no SGPG was detected in confluent HBMECs (Fig. 6).

Neutral GSL Composition of HBMECs

GSL structures were verified by immunostaining with specific anti-neutral GSL antibodies on thin-layer chromatograms. Figure 7 shows the orcinol-stained HPTLC pattern of the neutral GSL fraction in HBMECs and HUVECs, indicating these endothelial cells comprise three major neutral GSLs including LacCer, Gb3, and Gb4. The structures of these neutral GSLs were confirmed by HPTLC/SIMS (data not shown) and the HPTLC-GSL overlay method using specific antibodies (Fig. 8). Negative SIMS mass spectra of neutral GLSs showed prominent dehydrogenated molecular ions $[M - H]^-$ that corresponded to GSL molecular species containing fatty acids with chain lengths ranging from C18:0 to C24:0 and C18 sphingenine. The band comigrating to LacCer showed the fragmented ions corresponding to ceramide (Cer) (m/z 536-m/z 648), Cer-monosaccharide (m/z 698-m/z 810), and Cer-disaccharide ($[M - H]^-$; m/z 860-m/z 972), resulting in Cer-Hex-Hex. The lower two bands showed the same fragment ions corresponding to Cer, Cer-monosaccharide, and Cer-disaccharide. In the band comigrating to Gb3, the terminal sugar was found to be hexose (Hex) (m/z 162), resulting in Cer-Hex-Hex-Hex ([M -

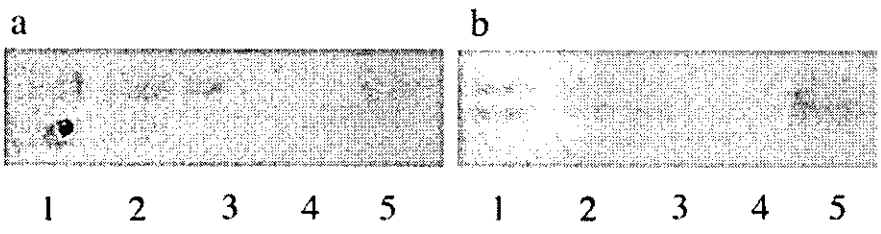

Fig. 8. HPTLC-overlay method with anti-Gb3 antibody (a) and anti-Gb4 antibody (b). Lanes 1–4: 1, .5, 0.1, 0.05 μg of authentic Gb3 (a) and Gb4 (b), respectively. Lane 5: neutral GSL fraction obtained from confluent HUVECs.

$H]^-$; m/z 1134). The band comigrating to Gb4 was Cer-tetrasaccharide and terminal sugar found to be *N*-acetylhexosamine (HexNAc) (m/z 203), resulting in Cer-Hex-Hex-Hex-HexNAc ($[M - H]^-$; m/z 1225-m/z 1337). Neither HBMECs nor HUVECs contained glucosyl ceramide or galactosyl ceramide, so far as HPTLC pattern. The amount of Gb3 in HBMECs was almost as twice that in HUVECs. No appreciable differences in neutral GSL quantity were observed before and after confluency.

DISCUSSION

It is difficult to guarantee that the cultured brain-derived ECs are really originated from ECs forming BBB. Such an assumption is made usually from elongated, fibroblast-like shape or increased resistance and limited passage of small molecules through monolayer of these cells, but conventional methods to isolate BMECs cannot escape contamination of ECs other than BMECs, namely, ECs from larger vessels lacking BBB properties. To solve this problem, we first carried out DNA microarray analysis to confirm expression of one of the most important barrier-specific genes, *mdr1* (Cordon-Cardo et al., 1989), in ECs used in the present study. Because we confirmed *mdr1* gene expression in HBMECs and its absence in HUVECs, the GSL content differences in HBMECs and HUVECs may partially reflect possible differences in cellular properties related to BBB function.

The most striking difference between GSL content of HBMECs and HUVECs is the amount of SGPG. This HNK-1 epitope-bearing GSL belongs to a novel class of acidic lipids present primarily in peripheral nerve tissues (Chou et al., 1986; Ariga et al., 1987). In mammalian CNS, sulfoglucuronosyl GSLs (SGGLs) including SGPG are known to be developmentally regulated, being expressed in embryonic forebrain and disappearing during the postnatal period (Schwarting et al., 1987), except in murine cerebellum (Chou and Jungalwala, 1988) and human optic nerve (Yoshino et al., 1993). Other than CNS parenchyma, we provided evidence that SGPG is an integral component of cultured bovine BMECs and demonstrated that SGPG is the only GSL whose concentration shows a wide fluctuation depending upon culture conditions and age (Kanda et al., 1994). Treatment of these cells with interleukin 1β (IL-1β) induced accumulation of SGPG (Kanda et al., 1995). In the present study, we found SGPG in HBMECs was much lower than that in HUVECs, and the SGPG content in both cells decreased markedly after confluency. Such marked fluctuations in SGPG expression, influenced by culture age, inflammatory cytokines, and the presence or absence of contact inhibition, may suggest a functional importance of this GSL as the surface receptor of ECs forming the BBB.

These changes in expression of SGPG may be due primarily to rapid upregulation and downregulation of glucuronyltransferase activity, probably triggered by endothelial cell–endothelial cell contact. COS-1 cells transfected with glucuronyltransferase-P cDNA (an enzyme involved in the biosynthesis of the HNK-1 epitope) (Seiki et al., 1999) and transformed into HNK-1-positive cells lost the tendency to aggregate and remained single cells (Kawasaki and Oka, 2001). The previous data and our findings indicate that the HNK-1 epitope, also known as an adhesion molecule, inhibits homophilic contact between HNK-1 epitope-bearing cells and is expressed mainly in single, proliferating cells. Because SGPG localized on BMECs acts as ligand for L-selectin expressed on the surface of circulating lymphocytes (Kanda et al., 1995) and anti-SGPG antibody (LT serum) possibly reacts with ECs forming the blood–nerve barrier and impairs their barrier function (Kanda et al., 1994, 1998), SGPG-rich proliferating ECs that repair injured barrier system may have more chance to be attacked by lymphocytes and antibodies; thus forming a vicious circle of inflammation.

The amounts of two major acidic GSLs, GM3 (NeuAc) and LM1, was also smaller in HBMECs than in HUVECs. Different from that of SGPG, the amount of GM3 (NeuAc) and LM1 was increased significantly after confluency in HBMECs. Neutral GSLs did not show any significant changes after confluency. The physiologic meaning of this difference is unknown; however, these dynamic changes in amounts of acidic GSLs including SGPG may be based on signaling systems triggered by endothelial cell–endothelial cell contact and might influence BBB integrity. The presence of neolacto-series gangliosides including NeuAc-nLcOse$_6$, NeuAc-nLcOse$_8$, and NeuAc-nLcOse$_{10}$ in HBMECs and HUVECs (Muthing et al., 1999) was confirmed using the HPTLC-overlay method and Far-Eastern blot/mass spectrometry. These minor species, however, did not show any difference between HUVECs and HBMECs.

Finally, the differences in GSL content observed in the present study and reported in previous studies are briefly discussed. HBMECs express a composition of